Regulation of intestinal epithelial intercellular adhesion and barrier function by desmosomal cadherin desmocollin-2

Arturo Raya-Sandino[a,†], Anny-Claude Luissint[a,†], Dennis H. M. Kusters[a], Vani Narayanan[b], Sven Flemming[a], Vicky Garcia-Hernandez[a], Lisa M. Godsel[c], Kathleen J. Green[c,d], Susan J. Hagen[e], Daniel E. Conway[b], Charles A. Parkos[a], and Asma Nusrat[a,*]

[a]Department of Pathology, University of Michigan Medical School, Ann Arbor, MI 48109; [b]Department of Biomedical Engineering, Virginia Commonwealth University, Richmond, VA 23284; [e]Department of Surgery, Beth Israel Deaconess Medical Center, Boston, MA 02115; [c]Departments of Pathology and Dermatology, Feinberg School of Medicine, Northwestern University, Chicago, IL 60611; [d]Robert H. Lurie Comprehensive Cancer Center of Northwestern University, Chicago, IL 60611

ABSTRACT **The role of desmosomal cadherin desmocollin-2 (Dsc2) in regulating barrier function in intestinal epithelial cells (IECs) is not well understood. Here, we report the consequences of silencing Dsc2 on IEC barrier function in vivo using mice with inducible intestinal–epithelial-specific *Dsc2* knockdown (KD) (*Dsc2*$^{ER\Delta IEC}$). While the small intestinal gross architecture was maintained, loss of epithelial Dsc2 influenced desmosomal plaque structure, which was smaller in size and had increased intermembrane space between adjacent epithelial cells. Functional analysis revealed that loss of Dsc2 increased intestinal permeability in vivo, supporting a role for Dsc2 in the regulation of intestinal epithelial barrier function. These results were corroborated in model human IECs in which Dsc2 KD resulted in decreased cell–cell adhesion and impaired barrier function. It is noteworthy that Dsc2 KD cells exhibited delayed recruitment of desmoglein-2 (Dsg2) to the plasma membrane after calcium switch-induced intercellular junction reassembly, while E-cadherin accumulation was unaffected. Mechanistically, loss of Dsc2 increased desmoplakin (DP I/II) protein expression and promoted intermediate filament interaction with DP I/II and was associated with enhanced tension on desmosomes as measured by a Dsg2-tension sensor. In conclusion, we provide new insights on Dsc2 regulation of mechanical tension, adhesion, and barrier function in IECs.**

Monitoring Editor
Alpha Yap
University of Queensland

Received: Dec 16, 2020
Revised: Feb 2, 2021
Accepted: Feb 9, 2021

INTRODUCTION

The intestinal epithelium resides at the interface of the intestinal lumen and underlying tissues and plays an essential role in fluid and nutrient absorption while also restricting pathogen access (Luissint *et al.*, 2016). Barrier properties of intestinal epithelial cells (IECs) are achieved by a series of intercellular junctions, including tight junction (TJ), adherens junction (AJ), and desmosomes (DMs), which are located along the lateral membrane (Laukoetter *et al.*, 2006). TJ and AJ comprise the apical junctional complex situated

This article was published online ahead of print in MBoC in Press (http://www.molbiolcell.org/cgi/doi/10.1091/mbc.E20-12-0775) on February 17, 2021.

†A.R-S. and A-C.L. contributed equally to this work.

Author contributions: A.R.-S. and A.-C.L. designed, performed experiments, analyzed, and interpreted data; A.R.-S. and A.-C.L. wrote and revised the manuscript; D.H.M.K., V.N., S.F., V.G.-H., and L.M.G. assisted with collecting data; K.J.G., S.J.H., D.C., and C.A.P. helped with design of experiments, provided resources, and edited the manuscript; A.N. supervised the study, designed experiments, provided resources, wrote, and edited the manuscript.

Competing interests: The authors declare no competing interests.

*Address correspondence to: Asma Nusrat (anusrat@umich.edu).

Abbreviations used: AJ, adherens junction; BSA, bovine serum albumin; CK8, Cytokeratin-8; DM, desmosome; DP, desmoplakin; *Dsc2*$^{ER\Delta IEC}$, *Villin*-Cre^{ERT2}-*Dsc2*$^{f/f}$; Dsc, desmocollin; Dsg, desmoglein; FRET, Föster resonance energy transfer; GAPDH, glyceraldehyde 3-phosphate dehydrogenase; IEC, intestinal epithelial cell; IF, intermediate filament; IMS, intermembrane space; KD, knockdown; NS, non-silencing control cells; NT, nontreated cells; PBS, phosphate-buffered saline; pDP, phosphorylated desmoplakins I/II at Ser2849; Pkp3, plakophilin 3; shRNA, short hairpin RNA; TBP, TATA-box–binding protein; TEER, transepithelial electrical resistance; TEM, transmission electron microscopy; TJ, tight junction.

in the most apical region of the lateral membrane. While TJs selectively regulate the paracellular movement of water, ions, and solutes, AJs mediate intercellular adhesion. Subjacent to the AJ are DMs that form "spot welds" between cells and function to strengthen cell–cell adhesion. By electron microscopy, DMs are visualized at the cell membrane as pairs of electron-dense disks longitudinally bisected at the intercellular space by a midline zipperlike structure. On the cytoplasmic side, desmosomal plaques anchor the protruding intermediate filaments (IF) to the membrane (Farquhar and Palade, 1963; Green and Simpson, 2007; Kowalczyk and Green, 2013; Nekrasova and Green, 2013; Cirillo, 2016). DMs are composed of transmembrane cadherin family members desmoglein (Dsg) and desmocollin (Dsc), which establish the cell–cell contact by associating their extracellular domains in the paracellular space. The cytoplasmic tails of these cadherins are linked to IFs by plaque proteins that include desmoplakins (DP), plakophilins, and plakoglobin (Holthofer *et al.*, 2007). While multiple isoforms of desmosomal cadherins (Dsg 1–4 and Dsc 1–3) are expressed in stratified complex epithelia, DMs in IEC monolayers are composed exclusively of Dsg2 and Dsc2. DMs have been implicated in controlling the strength of intercellular adhesion in complex epithelia such as the skin and the heart, thereby playing an important role in maintaining tissue integrity. DMs resist forces exerted on tissues that undergo mechanical stress (Baddam, Arsenovic *et al.*, 2018; Price, Cost *et al.*, 2018). The importance of tissue architecture maintenance by DMs is highlighted in patients with diseases of organs subjected to high mechanical forces such as the skin and the heart. DMs in these organ systems are dysfunctional in individuals with inherited mutations or by the generation of autoimmune antibodies, resulting in skin epithelial blistering and heart muscle dysfunction (Kottke *et al.*, 2006). Paradoxically, DMs also generate tensile forces by anchoring cadherins to the contractile IF-cytoskeleton (Broussard, Yang *et al.*, 2017; Charras and Yap, 2018). However, mechanisms by which desmosomal cadherins sense mechanical forces to support intercellular adhesion and tissue integrity remain unclear. In this respect, recent studies using Föster resonance energy transfer (FRET)-based tension sensors (TS) revealed that desmosomal proteins Dsg2 and DP I/II contain force-absorbing function. Dsg2 has been reported to experience low or higher mechanical tension levels in resting cells and during cardiomyocyte contraction, respectively. DP I/II becomes mechanically loaded when cells are exposed to external forces (Broussard, Yang *et al.*, 2017; Baddam, Arsenovic *et al.*, 2018; Price, Cost *et al.*, 2018). Interestingly, DP I/II tension properties are modulated by its association with IF-cytoskeleton. In fact, cell–cell forces depending on DP I/II-IF interactions are increased by mutating Ser2849 in the DP C-terminus, which strengthens the interaction of DP I/II to the IF-cytoskeleton (Broussard, Yang *et al.*, 2017).

Whereas Dsg2-mediated desmosomal adhesion has been reported to contribute to the intestinal epithelial barrier function (Schlegel *et al.*, 2010; Ungewiss *et al.*, 2017; Gross *et al.*, 2018), the role of Dsc2 in mediating these functions remains to be defined. In the current study, we examined the role of Dsc2 in intercellular junction formation and stability, as well as barrier function of IECs by using mice with IEC-specific inducible down-regulation of Dsc2, *Villin*-Cre^{ERT2} mice (*Dsc2*$^{ER\Delta IEC}$) (el Marjou *et al.*, 2004; Flemming, Luissint *et al.*, 2020). We found that loss of IEC-Dsc2 resulted in decreased DM size and increased intermembrane space (IMS) within DMs and led to intestinal epithelial barrier defects in vivo. Using a calcium switch assay to study intercellular junction assembly, we observed that in the absence of Dsc2, the incorporation of Dsg2 was delayed at the plasma membrane without impairing recruitment of the AJ protein, E-cadherin. To determine the mechanism by which Dsc2 silencing regulates IEC intercellular adhesion, we explored cadherin-based tensile forces at the AJ and DMs. IEC-Dsc2 knockdown (KD) led to altered mechanical tension force on the Dsg2-TS during intercellular junction assembly, without influencing the E-cadherin-TS. Interestingly, loss of Dsc2 also resulted in increased DP I/II protein and promoted association of the IF-cytoskeleton to DP I/II, which has been related to enhanced intercellular forces. Taken together, our findings identify an important role for Dsc2 in regulating intestinal epithelial intercellular junction formation, adhesion, and epithelial barrier function by controlling desmosomal tensile forces.

RESULTS

Inducible-targeted deletion of Dsc2 in IECs influences DM structure

To identify the contribution(s) of Dsc2 in regulating intestinal epithelial intercellular adhesion and barrier function, we generated mice with IEC-specific tamoxifen-inducible deletion of Dsc2 (*Dsc2*$^{ER\Delta IEC}$) (Flemming, Luissint *et al.*, 2020). *Dsc2* mRNA was specifically down-regulated in IECs in the small intestine and unaffected in other tissues including the heart (Figure 1, A and B). Additionally, specific knockdown of Dsc2 protein in IECs in the ileum was confirmed by Western blot analysis and immunofluorescence labeling of Dsc2 (Figure 1, C and D). IEC-Dsc2 deficiency did not alter protein levels of Dsg2 and E-cadherin in *Dsc2*$^{ER\Delta IEC}$ (Figure 1C) nor their subcellular localization along the crypt-villus axis in the small intestine as compared with *Dsc2*$^{f/f}$ control littermate mice (Figure 1D). Similar results were obtained in the colon of these mice which did not show a significant change in Dsg2 and E-cadherin protein in *Dsc2*$^{ER\Delta IEC}$ compared with *Dsc2*$^{f/f}$ mice (Supplemental Figure S1B) (Flemming, Luissint *et al.*, 2018). Furthermore, histologic analysis of hematoxylin and eosin-stained tissue sections of the small bowel, including ileum, revealed no gross alterations in mucosal architecture in *Dsc2*$^{ER\Delta IEC}$ mice and *Dsc2*$^{f/f}$ (Supplemental Figure S1A). We next determined whether Dsc2 loss in IECs modified the ultrastructural organization of DMs in the ileum by electron microscopic analysis. As depicted in the schematic in Figure 2A (top panel), multiple DMs are located beneath TJ and AJ in IECs. Desmosomal ultrastructure was evaluated by measuring width, length, and IMS, which is the intercellular space between two desmosomal plaques of adjacent cells (Figure 2A, bottom panel) (Gross *et al.*, 2018). In control *Dsc2*$^{f/f}$ mice, desmosomal spot welds between adjacent IECs were visualized as electron-dense plaques that consist of two electron-dense regions separated by a clear zone (IMS), similar to previously reported studies (Figure 2B) (Farquhar and Palade, 1963; Green and Simpson, 2007; Kowalczyk and Green, 2013; Nekrasova and Green, 2013; Cirillo, 2016). Dsc2 deficiency resulted in DM morphologic abnormalities compared with *Dsc2*$^{f/f}$ mice (Figure 2B). Specifically, the width and length of desmosomal plaques were significantly diminished, and the IMS was increased in *Dsc2*$^{ER\Delta IEC}$ mice compared with control *Dsc2*$^{f/f}$ (Figure 2C). Noteworthy, as indicated in Supplemental Figure S2, TJ and AJ length was similar in *Dsc2*$^{ER\Delta IEC}$ and *Dsc2*$^{f/f}$ mice. The IMS at AJ was slightly increased in *Dsc2*$^{ER\Delta IEC}$ mice, whereas evaluation of TJs in the transmission electron microscopy (TEM) images revealed apical electron-dense areas of close membrane apposition in both *Dsc2*$^{ER\Delta IEC}$ and *Dsc2*$^{f/f}$ mice. Altogether, these findings strongly indicate that Dsc2 significantly contributes to DMs organization and modulates to a lesser extend AJ adhesion structures in the simple intestinal epithelium. Thus, for the current study, we focused on analyzing DMs in Dsc2 KD cells.

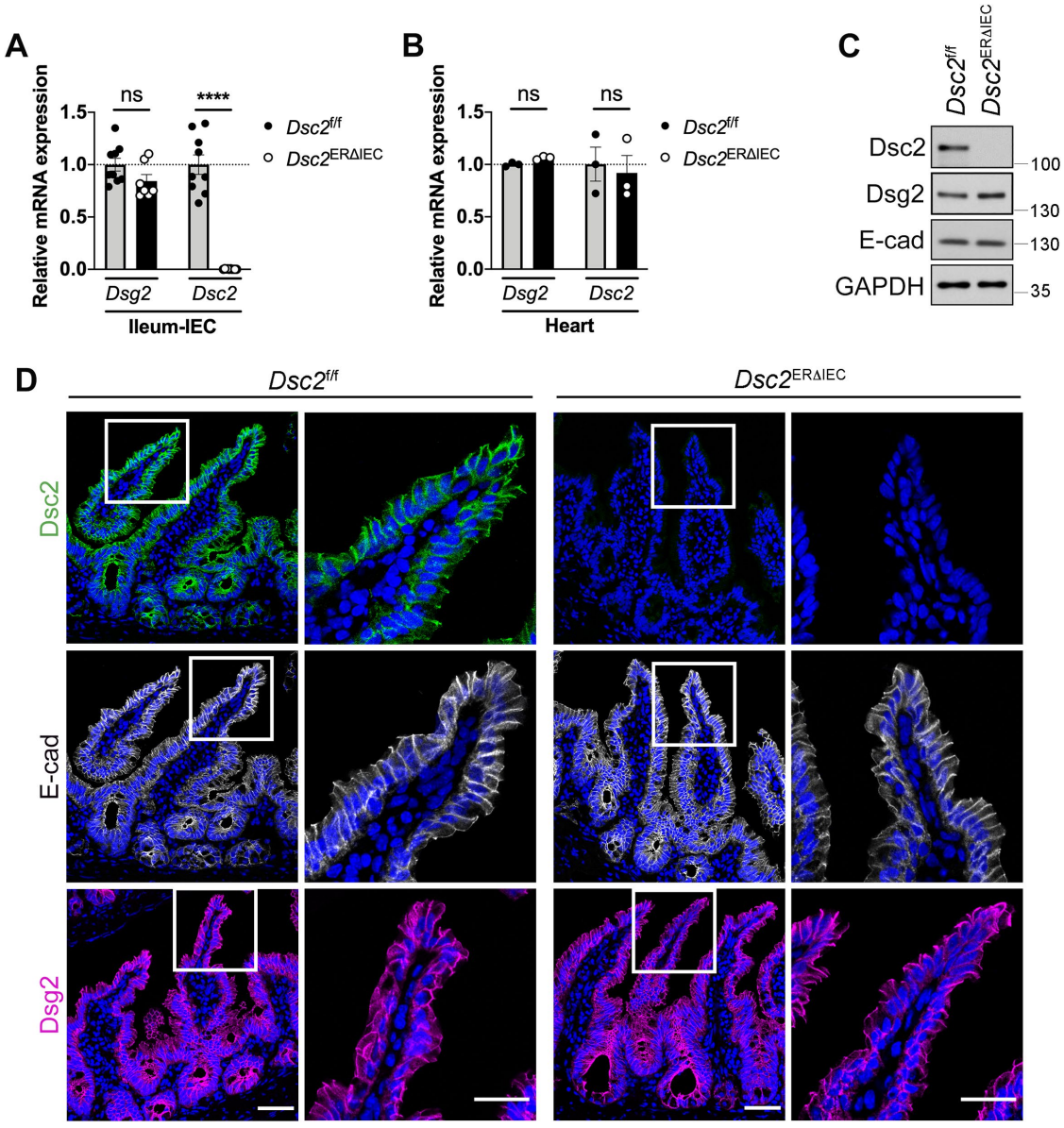

FIGURE 1: Loss of Dsc2 in IECs did not alter intestinal mucosal architecture as well as Dsg2 and E-cadherin expression. Intestinal epithelial-specific deletion of Dsc-2 was confirmed in the ileum of *Dsc2*$^{ER\Delta IEC}$ mice and control littermates *Dsc2*$^{f/f}$ treated with tamoxifen and analyzed 30 d later. (A) Loss of *Dsc2* mRNA expression, but not of *Dsg2* mRNA in ileal IECs isolated from *Dsc2*$^{ER\Delta IEC}$ mice or control *Dsc2*$^{f/f}$. Points represent values from an individual mouse. Graph combines values obtained from two independent experiments with a total of seven to nine mice per group. Data are means ± SEM. ****$p < 0.0001$; significance is determined by two-tailed Student's t test. (B) Expression of *Dsc2* and *Dsg2* mRNA is unchanged in the heart that does not express Villin, confirming tissue-specificity of Dsc2 depletion. Results are representative of two independent experiments. Points represent values from an individual mouse. Differences are not significant (ns) by two-tailed Student's *t* test. (C) IECs were isolated from the ileum of *Dsc2*$^{ER\Delta IEC}$ and *Dsc2*$^{f/f}$ mice. Protein were separated by SDS–PAGE and visualized by immunoblotting with antibodies against Dsg2, Dsc2, E-cadherin, and GAPDH as loading control. Representative Western blot images showing loss of Dsc2 in the ileal epithelium in *Dsc2*$^{ER\Delta IEC}$ mice while Dsg2 and E-cadherin expression is unaltered. (D) Representative images of ileal tissue sections from tamoxifen-treated *Dsc2*$^{ER\Delta IEC}$ and *Dsc2*$^{f/f}$ mice stained with anti-Dsc2, anti-Dsg2 or anti-E-cadherin antibodies and DAPI as a nuclear counterstain. Dsc2 expression is absent in ileal crypt-villus epithelial cells of *Dsc2*$^{ER\Delta IEC}$ mice with no change in Dsg2 and E-cadherin expression. Scale bars are 50 µm.

IEC-Dsc2 deficiency compromises epithelial barrier function in vivo and in vitro

Since DMs contribute to epithelial barrier properties, we next investigated the functional consequences of Dsc2 loss on intestinal epithelial barrier function in vivo. FITC-dextran (4-kDa molecular weight) was injected into the lumen of an exteriorized fully vascularized ileal loop and paracellular flux of FITC-dextran across the intestinal epithelium into the blood was measured in *Dsc2*$^{ER\Delta IEC}$ and control *Dsc2*$^{f/f}$ mice (Figure 3A) (Monteiro *et al.*, 2013; Wang *et al.*, 2015; Flemming, Luissint *et al.*, 2018). Dsc2 deficiency in IECs resulted in a significant increase in FITC-dextran flux in *Dsc2*$^{ER\Delta IEC}$ compared with control *Dsc2*$^{f/f}$ mice

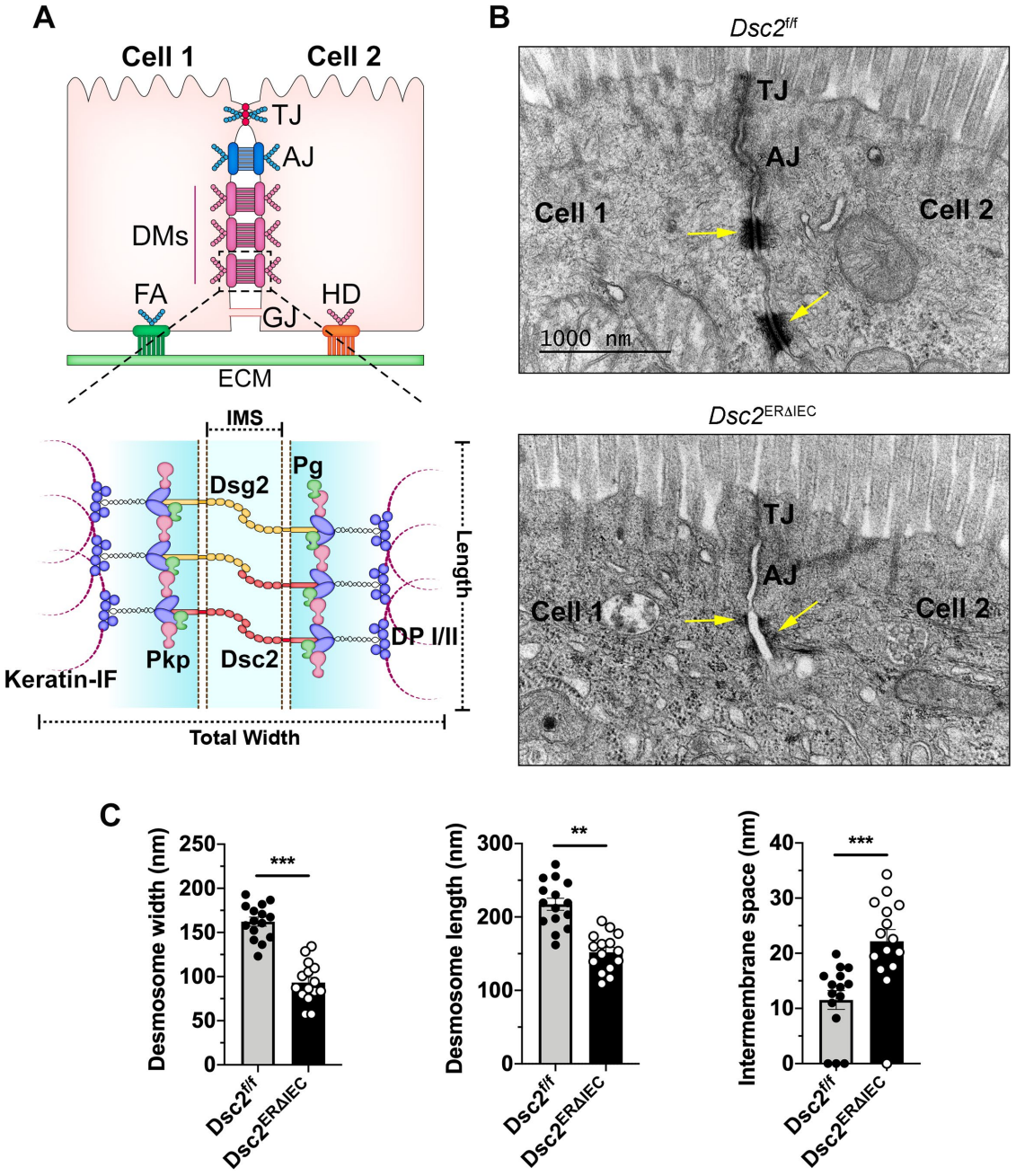

FIGURE 2: Loss of IEC Dsc2 is associated with reduced DM size and increased IMS. (A) Top panel: schematic diagram showing the localization of intercellular junctional complexes between adjacent IECs. TJ, tight junction; AJ, adherens junction; DM, desmosome; GJ, gap junction; FA, focal adhesion; HD, hemidesmosome. Bottom panel: schematic representation of DM complex depicting total width, length, and IMS. Pkp, plakophilin; DP I/II, desmoplakins I/II; Pg, plakoglobin. (B) TEM images of DM structure (arrows) in the terminal Ileum of *Dsc2*$^{ER\Delta IEC}$ mice compared with littermate *Dsc2*$^{fl/fl}$ controls. The absence of Dsc2 resulted in DM structural changes that were shorter and had increased IMS. (C) Histograms represent total width, length, and IMS of DM measured from EM images from *Dsc2*$^{f/f}$ and *Dsc2*$^{ER\Delta IEC}$ mice. DM width was calculated by subtracting the IMS from the total width measurement. Five TEM images were analyzed and the first most apical DM per image was measured. Histograms show the mean ± SEM. Points represent values from individual DM in three mice per group (15 images/15 DMs). Significance was determined by two-tailed Student's *t* test. $^{**}p < 0.01$, $^{***}p < 0.001$.

indicating a nonredundant and critical role for Dsc2 in epithelial barrier function in vivo (Figure 3B). These findings were corroborated in vitro using model human IECs. Dsc2 was down-regulated in a model IEC line SKCO-15 by Dsc2 shRNA viral transduction (SKCO-15 Dsc2 KD cells) and compared with control cells transduced with a scrambled control nonsilencing (NS) shRNA. In line with the in vivo findings, KD of Dsc2 in SKCO-15 cells did not alter the expression of Dsg2 and E-cadherin proteins (Figure 3C). Furthermore, epithelial barrier function analysis revealed decreased transepithelial electrical resistance (TEER) that paralleled the increased paracellular flux to 4-kDa FITC-dextran in Dsc2 KD cells (Figure 3, D and E). Taken together, these observations

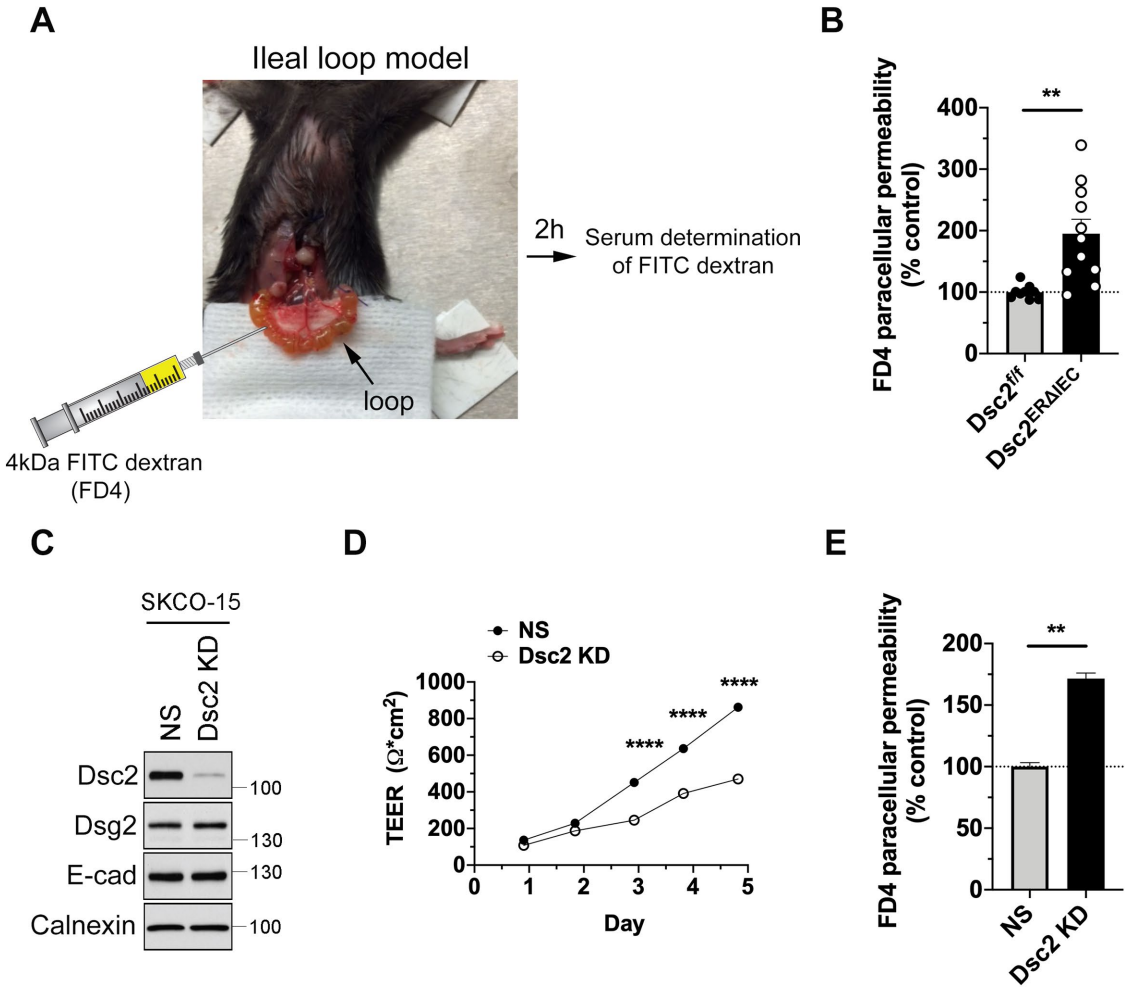

FIGURE 3: Loss of Dsc2 resulted in epithelial barrier dysfunction in vivo and in vitro. (A) Image of the ileal loop model used to quantify intestinal epithelial permeability to 4-kDa FITC-dextran in vivo in *Dsc2*$^{ER\Delta IEC}$ mice vs. *Dsc2*$^{f/f}$ controls. A 4-cm length of ligated ileal loop was exteriorized without disruption of blood supply following which a solution of 4-kDa FITC-dextran was administrated into the intestinal lumen. The ileal loop was placed back in the peritoneal cavity and at 2 h postinjection of FITC-dextran; serum concentrations of FITC were determined at 488 nm using a microplate spectrophotometer. (B) Dsc2 depletion resulted in increased intestinal permeability to 4-kDa FITC-dextran in vivo. Histograms show the mean ± SEM and points represent values from an individual mouse (9–11 mice per group). Data are combined from two independent experiments. Significance is determined by two-tailed Student's *t* test. $^{**}p < 0.01$. (C) Expression of Dsc2 in protein lysates from SKCO-15 cells transduced with shRNA-induced KD of Dsc2 (Dsc2 KD) was compared with nonsilencing shRNA control cells (NS). Western blot images are representative of at least three individual experiments and show KD of Dsc2, whereas the expression of E-cadherin and Dsg2 was unchanged. Calnexin was used as loading control. (D) TEER of cell monolayers from SKCO-15 Dsc2 KD cells vs. NS control was determined every day after cell seeding for 5 d. At day 5, TEER was reduced by twofold in SKCO-15 Dsc2 KD cells in comparison with control. Results show the mean ± SEM and are representative of four individual experiments, each one assayed in four technical replicates. Statistical analysis was done with two-way ANOVA, followed by Tukey´s posttest. $^{****}p < 0.0001$. (E) Paracellular flux of 4-kDa FITC-dextran across cell monolayers from SKCO-15 Dsc2 KD and NS control cells. FITC-dextran flux was significantly increased in SKCO-15 Dsc2 KD cells. Results show the mean ± SEM and are representative of four individual experiments, each one assayed in four technical replicates. Statistical analysis was done with two-tailed Student's *t* test. $^{**}p < 0.01$.

support the importance of Dsc2 in controlling the IEC barrier function.

Loss of Dsc2 impairs IECs intercellular adhesion

To further determine the mechanism by which Dsc2 regulates IEC barrier properties, we first investigated whether the loss of Dsc2 affects intercellular adhesive strength. Confluent SKCO-15 Dsc2 KD and control epithelial monolayers were subjected to a well-established dispase assay in which cell monolayers were detached from the extracellular matrix using protease dispase II treatment followed by mechanical stress to induce fragmentation of the monolayer. A higher number of fragments indicates weaker intercellular cell cohesion. Loss of Dsc2 resulted in an increased number of cell fragments compared with control cells (Figure 4, A and B). Similar results were obtained with another human model IEC line, Caco-2-BBE (Supplemental Figure S3). These observations support a role for Dsc2 in controlling IEC intercellular adhesion strength.

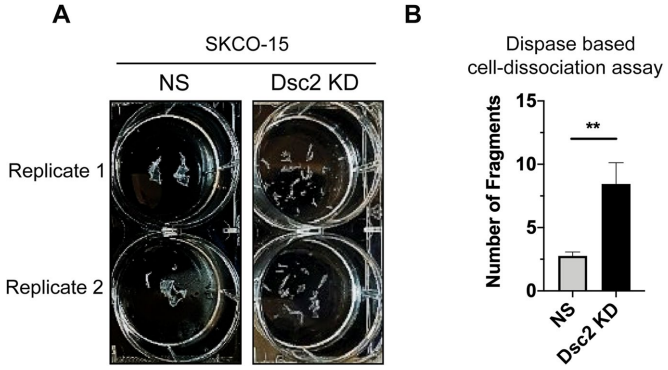

FIGURE 4: KD of Dsc2 in human model IECs resulted in reduced intercellular adhesion. (A) SKCO-15 cell monolayers with KD for Dsc2 vs. control NS were subjected to a dispase II-based mechanical cell dissociation assay to induce monolayer fragmentation as a readout of cell–cell adhesion. (B) Depletion of Dsc2 resulted in significantly increased epithelial monolayer fragmentation suggesting impaired cell–cell adhesion. Results show the mean ± SEM of data from three individual experiments, each one assayed in two technical replicates. Statistical analysis was done with two-tailed Student's *t* test. $^{**}p < 0.01$.

Dsc2 regulates DM complex formation without affecting E-cadherin targeting to the assembling AJ

Intercellular junctional complexes are dynamic structures that assemble and disassemble in response to various stimuli, such as proinflammatory mediators or mechanotransduction signals, that modify the strength and distribution of cell junction proteins (Andrews *et al.*, 2018; Charras and Yap, 2018). Junctional protein remodeling is required to maintain epithelial barrier function and epithelial homeostasis. Cadherins have been reported to play an important role in this process by controlling the assembly of intercellular junction protein complexes and their association with the cytoskeleton. For example, E-cadherin promotes not only AJ but also TJ and DM formation (Gumbiner *et al.*, 1988). E-cadherin facilitates the recruitment of Dsg2 and plakophilin3 to nascent DMs (Michels, Buchta *et al.*, 2009; Gosavi, Kundu *et al.*, 2011; Shafraz, Rubsam *et al.*, 2018). Conversely, silencing of desmosomal cadherin Dsg3 delays E-cadherin targeting to form junctions (Tsang *et al.*, 2012), indicating that DMs are significant regulators for AJ assembly. Given the relationship between AJ and DM, we next determined whether Dsc2 contributes to AJ and DM assembly using a calcium switch assay (Ivanov *et al.*, 2007). Dsc2 KD SKCO-15 monolayers or control cells (NS) were subjected to calcium depletion in low calcium medium (1 μM Ca^{2+}), resulting in cell–cell junction disassembly that is associated with the internalization of junctional proteins into intracellular vesicles (Ivanov *et al.*, 2005). Restoring extracellular calcium in cell medium (1.8 mM) promotes synchronized intercellular junction assembly. As shown in Figure 5A, calcium repletion in cell medium resulted in the development of epithelial barrier function as a readout of the intercellular junction assembly. TEER measurements to examine barrier function revealed that Dsc2 KD cells had lower TEER values compared with NS control cells over the entire course of junctional formation (Figure 5A). Thus, we next analyzed the incorporation of Dsg2 and E-cadherin into intercellular junctions after calcium depletion and repletion (Figure 5B). As shown in the en face confocal microscopy images and histograms depicting fluorescence intensity at plasma membrane (Figure 5, B and C), Dsg2 and E-cadherin were detected at intercellular contacts in both control and Dsc2 KD cells in nontreated (NT) monolayers. Although Dsg2 was visualized at intercellular contacts 60 min after extracellular calcium repletion in control cells expressing Dsc2, Dsg2 was still barely detected at cell borders at 180 min postcalcium repletion in Dsc2 KD cells (Figure 5, B and C). These findings suggest that loss of Dsc2 results in delayed targeting of Dsg2 to the intercellular junction during assembly after calcium switch. In contrast, E-cadherin was visualized at intercellular contacts in both control and Dsc2 KD cells over the entire course of junction formation after calcium repletion suggesting that E-cadherin localization at the lateral junctional membrane was not impaired by Dsc2 loss (Figure 5, B and C). All together these observations indicate that Dsc2 contributes to DM organization in IECs in vitro and its deficiency alters primarily DM assembly corroborating in vivo results obtained with $Dsc2^{ER\Delta IEC}$ and $Dsc2^{f/f}$ mice (Figure 2B and Supplemental Figure S2).

Dsc2 silencing increased desmosomal mechanical tension

Previous experiments have shown that AJ proteins, E-cadherin and α-catenin as well as desmosomal proteins Dsg2 and DP I/II, can resist mechanical forces to support intercellular adhesion and tissue integrity (Borghi, Sorokina, Shcherbakova *et al.*, 2012; Tornavaca *et al.*, 2015; Acharya *et al.*, 2017; Baddam, Arsenovic *et al.*, 2018; Price, Cost *et al.*, 2018). Therefore, we determined if Dsc2 loss modulates tension forces that are exerted on AJ and DM during junctional assembly after calcium switch by using specific FRET-based molecular TS that have been previously validated for E-cadherin (E-cad TS) and Dsg2 (Dsg2 TS) (Figure 6A) (Borghi, Sorokina, Shcherbakova *et al.*, 2012; Baddam, Arsenovic *et al.*, 2018). Dsg2-mediated DM tension was analyzed in NT monolayers, after calcium depletion and at 180 min after calcium repletion, which corresponds to the time when Dsg2 is targeted into the lateral junctional plasma cell membrane (Figure 5B). The untreated Dsc2 KD and NS monolayers exhibited the same Dsg2 TS FRET signal at plasma membrane. At time 0 of calcium repletion, the Dsg2 TS fluorescence signal was detected inside the cells, indicating Dsg2 internalization. Of note, some cells displayed Dsg2 TS at the cell membrane, which might be due to previously reported calcium-independent superadhesive properties of DM (Mattey and Garrod, 1986; Kimura *et al.*, 2007). At 180 min after calcium repletion, Dsg2 TS exhibited a significant decrease in FRET signal that correlates with higher tension forces across DM in the absence of Dsc2 compared with NS control cells (Figure 6, B and C). These observations indicate that loss of Dsc2 is associated with a change in Dsg2-mediated tension on DMs during intercellular junction assembly. Interestingly, at 180 min after calcium repletion, the AJ tension forces were unaffected as assessed by using an E-cad TS (Supplemental Figure S4), corroborating that loss of Dsc2 did not impair E-cadherin assembly in AJ (Figure 5B). Taken together, these results support a role of Dsc2 in controlling DM-mediated mechanical tension in IECs during junction formation.

Dsc2 loss is associated with change in DP I/II phosphorylation

DP I/II is a desmosomal scaffold protein (200–250 kDa) that generates tension force across DM by linking IF-cytoskeleton to desmosomal cadherins (Broussard, Yang *et al.*, 2017; Price, Cost *et al.*, 2018). Phosphorylation of DP I/II at Ser2849 has been reported to regulate DP I/II association with IF-cytoskeleton. A phosphorylation-deficient DP I/II generated by substitution of Ser2849 with Gly2849 enhanced interaction of DP I/II C-terminus with IF-cytoskeleton and increased intercellular tension force (Godsel, Hsieh, Amargo *et al.*, 2005; Broussard, Yang *et al.*, 2017). Since Dsc2 loss was associated with higher intercellular tension force compared with control cells at

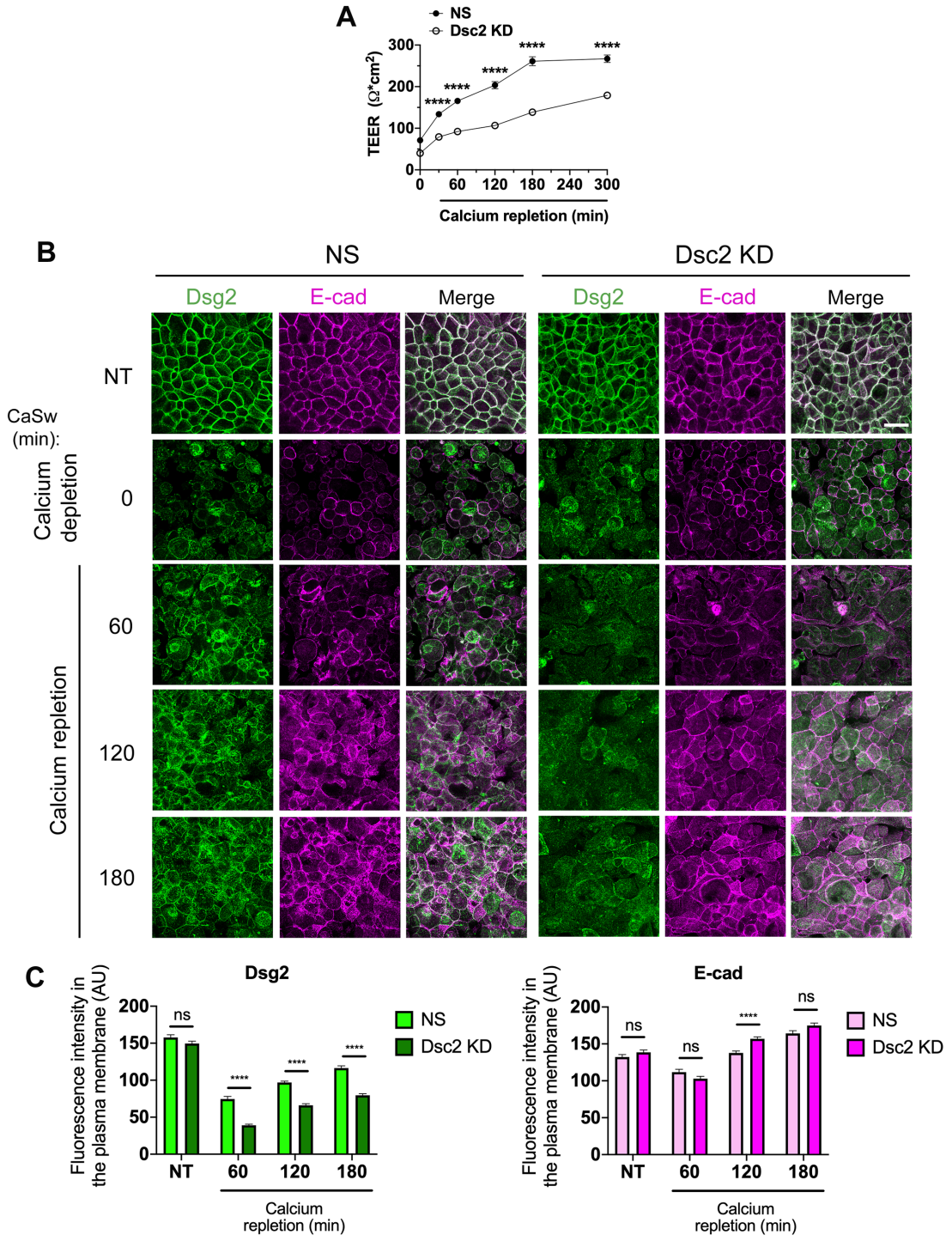

FIGURE 5: Dsc2 KD resulted in delayed recruitment of Dsg2 but not E-cadherin to the plasma membrane after calcium switch-induced cell junction assembly. Confluent monolayers of SKCO-15 cells KD for Dsc2 (Dsc2 KD) or control (NS) were transferred to low calcium media for 20 h (time 0), then cell monolayers were incubated in calcium-containing medium to induce intercellular junction re-assembly. (A) TEER was monitored over the course of calcium repletion ($t = 0$ up to 300 min). Results show the mean ± SEM and are representative of two individual experiments (two independent viral transductions) with a total of 12 technical replicates per condition. Statistical analysis was done with two-way ANOVA followed by Sidak´s posttest. ****$p < 0.0001$. (B) Confocal microscopy images of Dsg2 (DM) and E-cadherin (AJ) in SKCO-15 Dsc2 KD cells vs. control (NS) in either nontreated (NT) confluent monolayers or after calcium switch (CaSw) at four time points (0, 60, 120, and 180 min). Images are representative of three independent experiments (two independent viral transductions) and 24 images were analyzed per time point. Scale bars are 40 µm. (C) Histograms show fluorescence intensity of Dsg2 (green) and E-cadherin (magenta) in the plasma membrane of NT cell monolayers and after calcium repletion in Dsc2 KD cells and controls. Results show the mean ± SEM of three independent experiments with a total of 24 images per condition. A total of 240 cell–cell contacts were analyzed for NS and Dsc2 KD cells in both histograms. Statistical analysis was done with two-tailed Student's t test; ns, not significant; ****$p < 0.0001$.

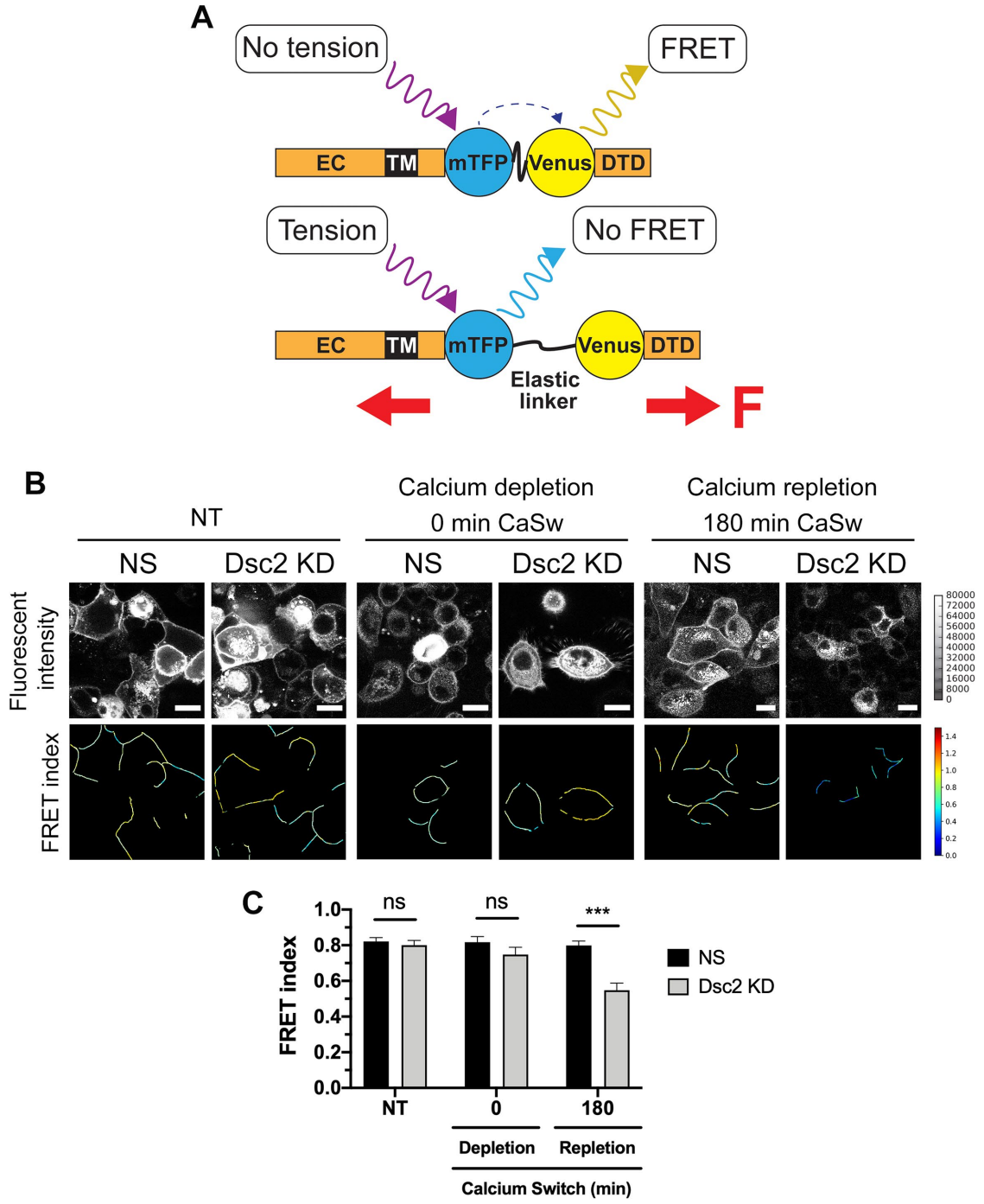

FIGURE 6: Loss of Dsc2 leads to enhanced tension forces on DM after calcium switch. (A) Schematic of the FRET-based molecular TS. The tension sensitive module (TS mod) consists of the mTFP/Venus FRET pair separated by an elastic linker. TS mod was inserted into the cytoplasmic domain of Dsg2, where it can sense forces transmitted between the transmembrane domain (TM) and Dsg-specific terminal domain (DTD). High and low FRET indices correspond to low and high tension, respectively. Under mechanical loading (red arrows), mTFP/Venus FRET pair is separated, and the FRET is reduced. EC: extracellular domain, F: force. (B) Representative color-coded images of three independent experiments, where cold and hot colors, respectively, indicate low and high levels of FRET index on Dsg2 TS mod. Monolayers expressing Dsg2 TS mod showed altered forces across DMs in SKCO-15 Dsc2 KD cells compared with the nonsilenced control (NS) during cell–cell junction recovery after calcium switch (CaSw) at two time points (0 and 180 min). (C) Histograms represent the average FRET index. Data are representative from three independent experiments. Statistical analysis was done with two-way ANOVA, followed by Tukey's posttest. *$p < 0.05$; ****$p < 0.0001$. Scale bar is 20 μm.

180 min, we analyzed DP I/II phosphorylation at Ser2849 (pDP) in these IECs. Surprisingly, knockdown of Dsc2 in human IEC line SKCO-15 resulted in a significant increase in DP I/II while the pDP/total DP I/II protein ratio was reduced in Dsc2 KD cells compared with control cells (Figure 7A). We further corroborated these findings by Western blot analysis of pDP and total DP I/II protein in the

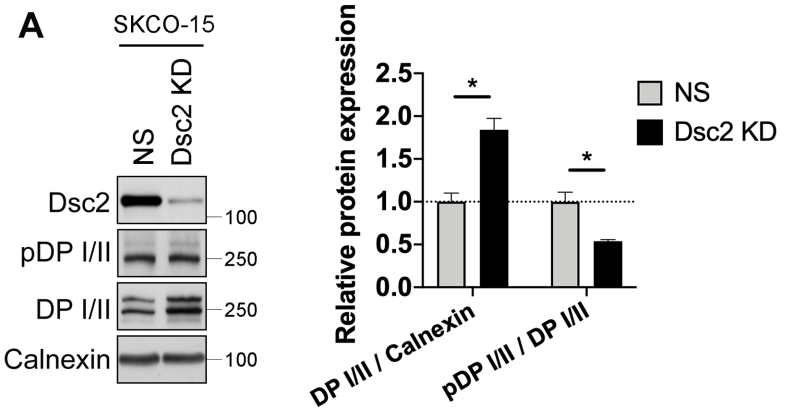
A
SKCO-15
NS
Dsc2 KD
Dsc2
pDP I/II
DP I/II
Calnexin
100
250
250
100
Relative protein expression
2.5
2.0
1.5
1.0
0.5
0.0
*
*
NS
Dsc2 KD
DP I/II / Calnexin
pDP I/II / DP I/II

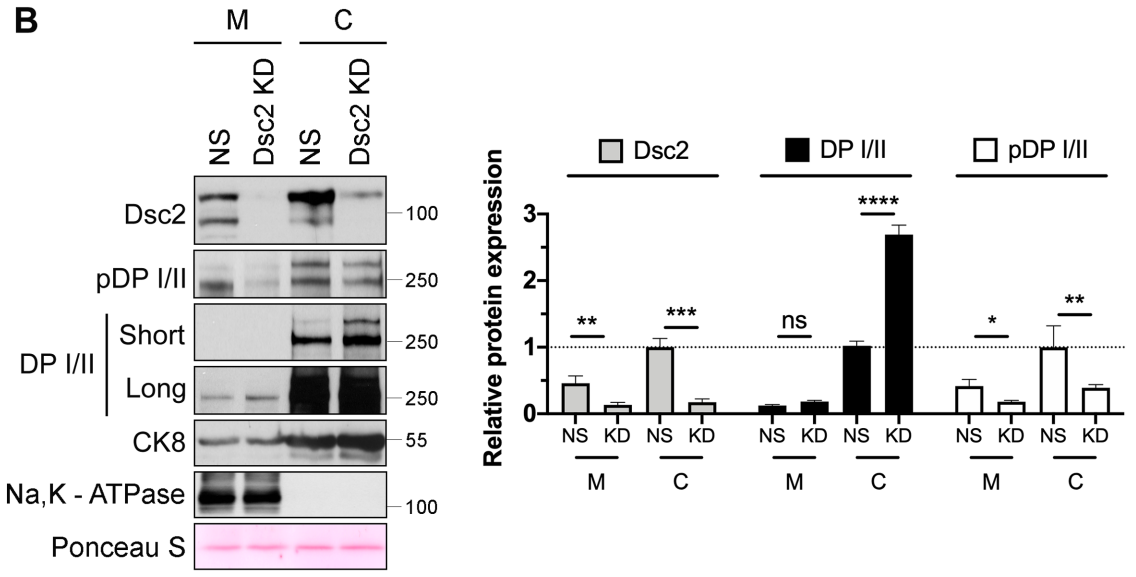
B
M
C
NS
Dsc2 KD
NS
Dsc2 KD
Dsc2
pDP I/II
DP I/II
Short
Long
CK8
Na,K - ATPase
Ponceau S
100
250
250
250
55
100
Dsc2
DP I/II
pDP I/II
Relative protein expression
3
2
1
0
**
***
ns
****
*
**
NS KD NS KD NS KD NS KD NS KD NS KD
M C M C M C

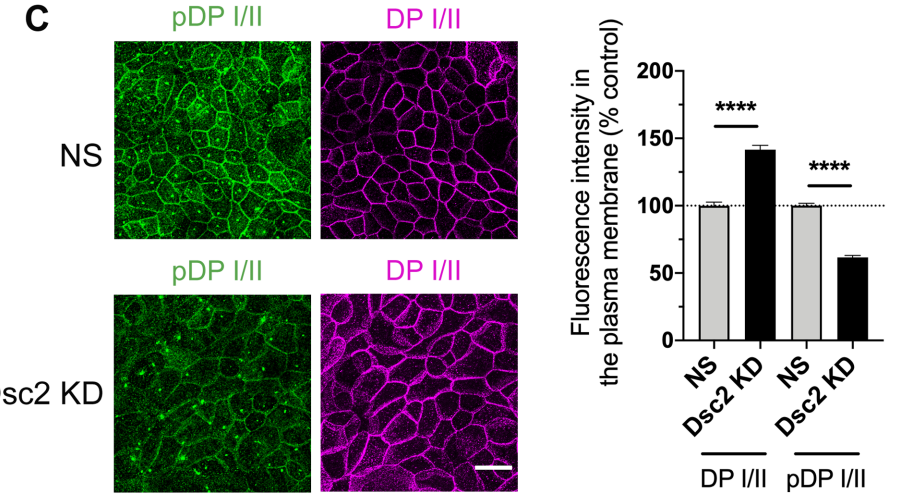
C
pDP I/II
DP I/II
NS
pDP I/II
DP I/II
Dsc2 KD
Fluorescence intensity in the plasma membrane (% control)
200
150
100
50
0
****
****
NS
Dsc2 KD
NS
Dsc2 KD
DP I/II
pDP I/II

Continues

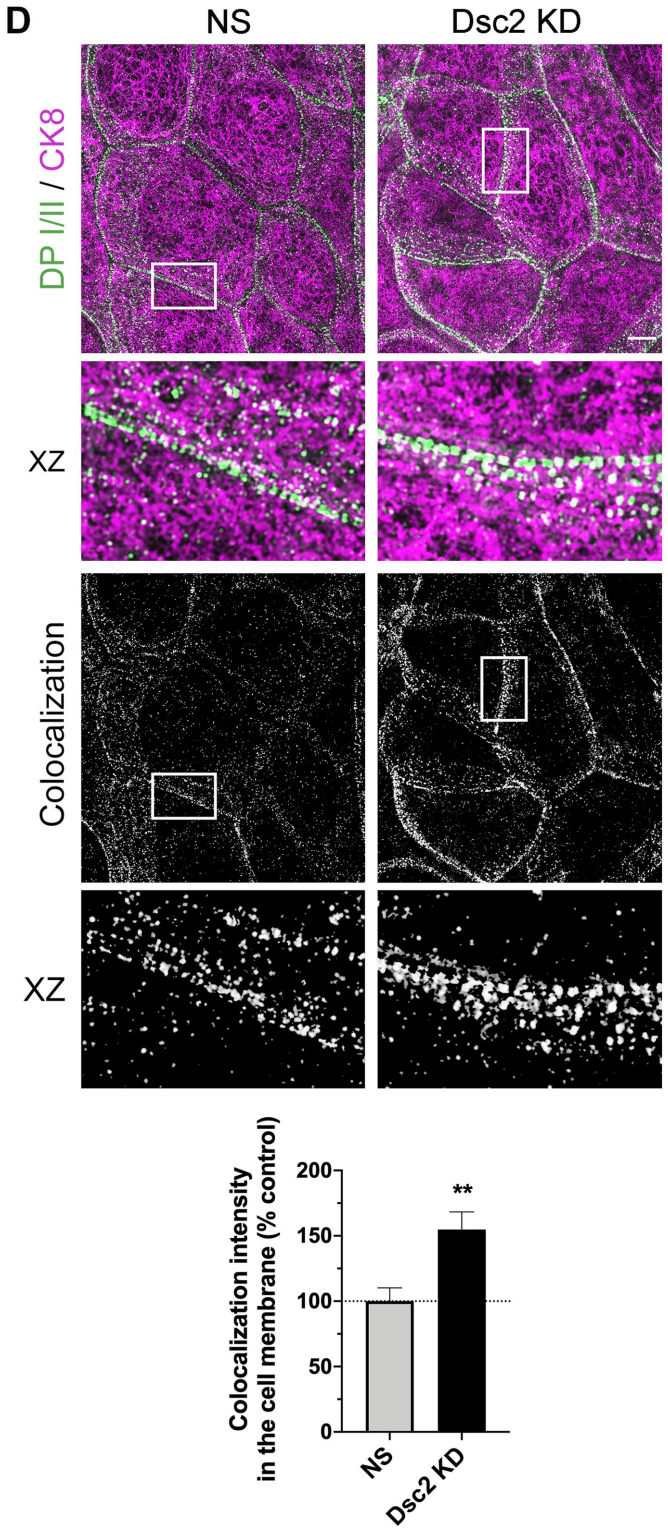

FIGURE 7: Dsc2 KD resulted in reduced DP I/II phosphorylation at Ser2849 and enhanced interaction of DP I/II to IF-cytoskeleton. (A) Left panel shows representative WB images of the expression of Dsc2, pDP, DP I/II, and calnexin (loading control) in whole cell lysates derived from SKCO-15 Dsc2 KD vs. NS cells. Bar graphs in the right panel show densitometric analysis of DP I/II expression normalized to calnexin and ratio pDP/ DP I/II. Data represent mean ± SEM of three independent experiments. Statistical analysis was done with two-tailed Student's *t* test. $*p < 0.05$. (B) Membrane and cytoskeletal fractions were isolated from Dsc2 KD and control SKCO-15 cells. The left panel shows representative WB images of the expression of Dsc2, pDP I/II, DP I/II, Na,K - ATPase (membrane marker), and CK8-IF marker in Dsc2 KD vs. NS cells. Ponceau S staining serves as a loading control for total protein normalization. The right panel shows the densitometry analysis. Data represent mean ± SEM of five independent experiments. Statistical analysis was done with wo-tailed Student's *t* test. ns, not significant; $*p < 0.05$.$**p < 0.01$; $***p < 0.001$; $****p < 0.0001$. (C) The left panel shows confocal microscopy images of pDP S2849 and DP I/II in SKCO-15 control (NS) vs. Dsc2 KD confluent monolayers. Scale bars are 40 µm. The right panel shows histograms depicting fluorescence intensity of DP I/II and pDP S2849 in the plasma membrane of KD confluent monolayers compared with NS control. Results show the mean ± SEM of three independent experiments, each one assayed in two technical replicates with a total of 24 images per condition. A total of 160 and 170 cell–cell contacts were analyzed for NS and Dsc2 KD cells, respectively. Statistical analysis was done with two-tailed Student's *t* test. $****p < 0.0001$. (D) Top panel, structured illumination microscopy images showing DP I/II (green) and CK8 (magenta) in SKCO-15 control (NS) and Dsc2 KD cells. Rectangles mark zoomed in areas. Scale bar is 5 µm. Bar graphs in the bottom panel show the fluorescence colocalization analysis, generated by Pearson´s correlation coefficients, between DP I/II and CK8 signals in the cell membrane in Dsc2 KD cells compared with NS cells. Results show the mean ± SEM of three individual experiments with a total of 12 images per condition, each one assayed in two technical replicates. For DP-CK8 interaction, a total of 70 and 75 cell–cell contacts were analyzed for NS and Dsc2 KD cells, respectively. Statistical analysis was done with two-tailed Student's *t* test. $**p < 0.01$.

membrane and cytoskeleton subcellular fractions in control and Dsc2 KD cells. Increased DP I/II protein but diminished pDP was identified in the cytoskeletal protein fraction in the absence of Dsc2 (Figure 7B). To gain further insights on Dsc2-dependent modulation of DP I/II interaction with IF-cytoskeleton, we analyzed the subcellular localization of DP I/II and pDP in confluent monolayers of control and Dsc2 KD cells (Figure 7C). The fluorescence intensity at the lateral junctional plasma membrane of pDP was reduced while the total amount of DP I/II in this compartment augmented in Dsc2 KD cells compared with controls (Figure 7C). Given that DP I/II phosphorylation at S2849 modulates IF-cytoskeleton interaction with DP I/II, and Dsc2 KD modulates DP I//II expression, we immunolocalized DP I/II and cytokeratin 8 by superresolution Structured Image Microscopy (SIM). Increased colocalization of DP I/II and cytokeratin 8 was observed in Dsc2 KD cells compared with control NS cells (Figure 7D). However, no significant change was detected in colocalization of DP I/II and F-actin (phalloidin staining) after loss of Dsc2 (Supplemental Figure S5). These findings support a role of Dsc2 in modulating DP I/II and cytokeratin association that in turn controls tension forces in DMs.

DISCUSSION

The intestinal epithelial barrier protects the body against harmful pathogens and substances from the external environment (Ma, 1997; Schmitz *et al.*, 2000; Laukoetter *et al.*, 2008). Intestinal barrier function is achieved by distinct epithelial junctional complexes encompassing TJ, AJ, and DMs that are organized along the lateral membrane between adjacent epithelial cells. In our study, acute silencing of Dsc2 in IECs altered DM structure, adhesion, and epithelial barrier function in vitro and in vivo. First, by TEM, we observed the presence of electron dense disk-shaped DM structures between adjacent ileal epithelial cells in mice that harbor IEC-specific Dsc2 deletion ($Dsc2^{ER\Delta IEC}$). However, Dsc2-deficient

Continued

DMs displayed reduced size and a larger intercellular space in comparison to those in ileal epithelial cells from control mice, supporting a role for Dsc2 in ensuring appropriate DM architecture. Of note, Dsc2 deficiency led to an enlarged intercellular space at the apical junctional complex but had no significant effect on AJ and TJ size and shape by TEM. Whether the loss of Dsc2 directly mediates this defect needs further investigation. Indeed, the absence of DP or treatment with the Pemphigus Vulgaris-related anti-Dsg3 antibody in keratinocytes has been reported to lead to altered AJ and TJ structures (Sumigray *et al.*, 2014). Therefore, it is tempting to speculate that Dsc2 might be essential not only for DM assembly but also for the proper formation of AJ and TJ complexes.

Dsc2 and Dsg2 are the only desmosomal cadherins expressed in the intestinal epithelium. In line with our findings, an in vitro study has reported a double knockdown of Dsc2 and Dsg2 in human adenocarcinoma DLD-1 cells using a CRISPR/Cas9 system. While double knockdown cells failed to form DMs, the re-expression of only Dsc2 in the double KD cells was sufficient to form DM-like structures (Fujiwara *et al.*, 2015). These findings implied a major role for Dsc2 in DM formation. Herein we report that Dsg2 expression is unchanged after Dsc2 depletion in both *Dsc2*$^{ER\Delta IEC}$ mice and IEC lines, and that DM formation was not completely abolished. In addition, it has been recently reported that Dsg2 depletion results in an altered DM structure in vivo suggesting a role for Dsg2 in DM formation (Koeser *et al.*, 2003; Gross *et al.*, 2018). Altogether these findings strongly suggest that either Dsc2 or Dsg2 alone are not sufficient for complete DM architecture in IEC. Furthermore, our results support an important role for intestinal epithelial Dsg2 in DMs organization in the absence of Dsc2.

Analysis of desmosomal cadherins suggests heterophilic interactions of Dsgs and Dscs in trans via a strand swap mechanism that is similar to classical cadherins (E-cadherin). In addition, a growing number of structural studies have provided evidence that both Dsg2 and Dsc2 are involved in homophilic and heterophilic interactions (Schlipp *et al.*, 2014; Harrison, Brasch *et al.*, 2016; Ungewiss *et al.*, 2018; Nie *et al.*, 2011; Shafraz, Rubsam *et al.*, 2018). Taken together, these observations are consistent with our findings and support a role for both Dsg2 and Dsc2 in orchestrating appropriate DM organization in simple IECs.

Second, given our observations that Dsc2 is necessary for DM formation in vivo and in vitro, we analyzed whether Dsc2 deficiency in IECs may alter intestinal barrier function. We found that Dsc2 deficiency in IECs resulted in increased intestinal epithelial permeability in vivo and in vitro. Our results are at odds with a recent study in which mice that harbor constitutive silencing of Dsc2 in IECs showed no difference in paracellular permeability compared with littermate controls (Gross *et al.*, 2018). However, the authors mentioned that in their experimental model, constitutive silencing of Dsc2 in IECs resulted in an accumulation of Dsg2-interacting protein Galectin 3 in the plasma membrane fraction, which could serve as a compensatory mechanism to prevent an intestinal barrier defect. Surprisingly, despite a compromised barrier function observed in *Dsc2*$^{ER\Delta IEC}$ mice, we did not detect spontaneous inflammation in the intestinal mucosa. These findings are in line with previous studies of unchallenged JAM-A null mice or intestinal epithelial specific loss of nonmuscle myosin IIA knockout mice that displayed increased intestinal permeability, without development of colitis, by up-regulation of adaptive immune response and production of TGF-β and antibacterial IgA to limit intestinal inflammation (Laukoetter, Nava *et al.*, 2007; Khounlotham *et al.*, 2012, Naydenov *et al.*, 2016). Given that we did not see increased mucosal immune cell infiltration or gross change in epithelial architecture in the ileum or colon of Dsc2$^{\Delta IEC}$ mice, it is likely that these mice have other mucosal protective mechanisms that maintain homeostasis.

In addition, the expression of E-cadherin and Dsg2 were not altered by the loss of Dsc2 in vivo and in vitro, which is consistent with previous reports indicating that IEC-specific silencing of Dsc2 did not impact either colon tissue architecture or the expression of E-cadherin and Dsg2 when compared with control cells (Gross *et al.*, 2018; Flemming, Luissint *et al.*, 2020).These findings are similar to a recent report showing that mice with intestinal epithelial knockout of β-actin have a leaky gut barrier without changes in assembly of epithelial apical junctions, and they do not develop spontaneous mucosal inflammation (Lechuga *et al.,* 2020). Here we show that Dsc2 deficiency resulted in increased paracellular permeability to macromolecules with size of 4-kDa FITC-dextran in vivo and in vitro. Although we did not observe major alteration in TJ structure, we cannot rule out that Dsc2 deficiency might modulate composition and distribution of claudins and therefore paracellular pore (< 8 Å) versus leak (> 100 Å) pathways (Zuo, Kuo *et al.,* 2020). Indeed, pore-forming claudin-2 is overexpressed during mucosal inflammation, and claudin-2 expression in vivo increases colonic epithelial permeability, yet transgenic mice overexpressing claudin-2 in the colon were protected from experimental colitis through positive regulation of colonocyte proliferation and immune tolerance that was proposed to limit the development of intestinal inflammation (Ahmad *et al.*, 2014). It is noteworthy that we recently reported that on intestinal mucosal injury, Dsc2 has a protective role in recovery from DSS-induced intestinal inflammation and biopsy-induced wound repair. In vitro analyses using human model IECs after Dsc2 KD revealed delayed epithelial cell migration and wound repair, which was associated with reduced cell-matrix traction forces, decreased integrin β1 and β4 protein, and altered activity of the small GTPase Rap1 compared with nonsilenced control cells (Flemming, Luissint *et al.*, 2020). All together our findings support the importance of Dsc2 in the maintenance of intestinal mucosal barrier function, homeostasis, and epithelial restitution after injury.

Third, here we show that loss of Dsc2 resulted in delayed incorporation of Dsg2 at intercellular contacts following calcium depletion and repletion in human IECs suggesting that Dsc2 contributes to the calcium-dependent DM assembly. Our findings corroborate numerous in vitro studies in epithelial cells. Indeed, a previous study used a modified calcium switch assay to enrich for nascent glycoprotein incorporation into the cell membrane to demonstrate that DM assembly occurs in two steps: in the first 30 min after calcium repletion, Dsc2-enriched vesicles were transported to the plasma membrane, where they were stabilized by a second wave of vesicles enriched with Dsg2 and associated armadillo proteins (Burdett and Sullivan, 2002). Similarly, Dsc2 but not Dsg2 has been reported necessary and sufficient to recruit DP I/II into DM-like puncta in MDCK cells that were seeded on micropatterned substrates of Dsc2aFc and/or Dsg2Fc (Lowndes *et al.*, 2014). In addition, double silencing of Dsg2 and Dsc2 in human intestinal adenocarcinoma DLD-1 cells resulted in a delayed barrier recovery detected by TEER measurement using a calcium switch assay. Dsg2-specific antibody was not able to inhibit epithelial barrier reformation (Ungewiss *et al.*, 2017). All together these findings imply a key role for Dsc2 in DM assembly and function in epithelial cells. Of note, we did not observe a delay in the recruitment of a TJ transmembrane protein JAM-A to lateral junctional complexes during calcium repletion in Dsc2 KD cells compared with NS control cells (data not shown). However, currently we cannot rule out that Dsc2 KD does not influence barrier-regulating TJ proteins such as claudins which will require further analysis. Interestingly, here we show that loss of Dsc2 did not delay the

reassembly of E-cadherin at the lateral plasma membrane after calcium repletion. Given that we observed an enlarged AJ intercellular space by TEM in the absence of Dsc2, the possibility that Dsc2 might influence other AJ-associated proteins is not excluded. There are numerous reports that have described E-cadherin and AJ to play a crucial role in DM formation (Yin and Green, 2004; Michels, Buchta *et al.*, 2009; Green *et al.*, 2010; Shafraz, Rubsam *et al.*, 2018). DM assembly has been described to be initiated at sites of E–cadherin-mediated adhesion and E-cadherin is required for efficient recruitment of Dsg2 and DP to intercellular cell–cell contacts (Shafraz, Rubsam *et al.*, 2018). Reciprocally, it has been reported that DM can regulate AJ formation. Indeed, loss of Dsg3 in keratinocytes resulted in impaired reintegration of E-cadherin and β-catenin into AJ after calcium switch (Tsang *et al.*, 2012). The same authors have reported a direct interaction between Dsg3 and E-cadherin that is dependent on plakoglobin and p120 which occurs in a calcium-dependent manner. In addition, Dsg3 was reported to modulate the activity of Src and its association with E-cadherin in AJ formation (Tsang *et al.*, 2012). Moreover, desmosomal component plakophilin 3 (Pkp3) has been shown to act as coordinator of DM and AJ assembly and maturation through its functional association with Rap1. Pkp3 deficiency causes disruption of an E-cadherin/Rap1 complex required for AJ sealing (Todorovic *et al.*, 2014). All together these data suggest an interconnection between desmosomal cadherins and AJs. Further investigations are needed to characterize the underlying molecular mechanisms that mediate cross-talk to cadherins in these intercellular junctions.

DMs were first described as spot welds formed between adjacent epithelial cells and have been well described for their critical role in maintaining the strength of intercellular adhesive bonds (Farquhar and Palade, 1963; Green and Simpson, 2007; Nekrasova and Green, 2013). Most studies have examined the role of desmosomal proteins in controlling adhesive and homeostatic properties in tissues subjected to high mechanical stress like skin and heart, suggesting that DMs can resist tensile forces that are either externally applied or produced through their interaction with the keratin-IF-cytoskeleton. Furthermore, it has been reported that mechanical forces that are exerted on AJs depend on actomyosin cytoskeleton contraction and can regulate barrier function (Borghi, Sorokina, Shcherbakova *et al.*, 2012; Tornavaca *et al.*, 2015; Acharya *et al.*, 2017). However, how desmosomal components sense mechanical forces and transduce signals to regulate intestinal epithelial barrier function remains unknown. It is tempting to speculate that keratin-IF might generate tension forces similarly to the actomyosin cytoskeleton and DMs might act as mechanosensory structures to regulate epithelial barrier function. This hypothesis is supported by studies predicting that IFs are subjected to mechanical tension (Ingber, 1993, 2003). IFs can become straight under stretch reaching strains up to 3.5× of the original length before breaking (Kreplak *et al.*, 2005; Fudge *et al.*, 2008). Also, keratin filament at cell–cell junctions is observed to be in alignment with filaments of the neighboring cells (Russell *et al.*, 2004). It is likely that IFs may generate tension and transmit mechanical signals between neighboring cells. Interestingly, using a DM-Dsg 2 TS, it was reported that Dsg2 supports mechanical tension in MDCK resting cells and during cardiomyocyte contraction (Baddam, Arsenovic *et al.*, 2018). In addition, Dsc2 KD in esophageal squamous carcinoma cell lines resulted in impaired intercellular adhesion and retraction of keratin-IFs (Fang *et al.*, 2014). Furthermore, DP I/II has been reported to support tension force across intercellular junctions when external stress was applied (Price, Cost *et al.*, 2018) and by cross-linking IFs to desmosomal cadherins (Broussard, Yang *et al.*, 2017). Here we show that KD of Dsc2 in IECs resulted in altered tensile forces at DM but not AJ during the formation of intercellular junctions after calcium switch by using DM-Dsg2 and AJ-E-cadherin FRET-based TS, respectively. Furthermore, Dsc2 deficiency resulted in enhanced colocalization of DP I/II and keratin-IFs at the cell membrane that paralleled with a significant decrease of pDP Ser2849 in cytoskeletal protein fraction. It was previously reported that overexpression of DP I/II or mutants that inhibits DP I/II phosphorylation at S2849 displayed higher cell–cell forces and cell stiffness through increased DP I/II association with IF-cytoskeleton (Broussard, Yang *et al.*, 2017). Our findings suggest that Dsc2 deficiency generates higher tensile forces at DMs driven by the association between DP I/II and IF-cytoskeleton.

Of particular interest to this study, several reports have shown the importance of Dsg2 in controlling intestinal barrier properties by facilitating DM assembly and modulating p38MAPK activity (Ungewiss *et al.*, 2017), EGFR localization, and Src-dependent activation (Ungewiss *et al.*, 2018). Dsg2 has also been proposed to function as a mechanosensor. This observation was made using a Dsg2 force sensor, which was expressed at the lateral membrane of living human cardiomyocytes and renal epithelial MDCK cells to directly measure mechanical forces across DMs (Baddam, Arsenovic *et al.*, 2018). The Dsg2 tension sensor experiments revealed that Dsg2 experiences mechanical forces of around 1.5 pN, similar to forces described for E-cadherin (Borghi, Sorokina, Shcherbakova *et al.*, 2012) and VE-cadherin (Conway *et al.*, 2017). Using atomic force microscopy, a recent study has reported Dsg2-specific binding events along the cell border on the surface of enterocytes with a mean unbinding force of around 30 pN (Ungewiss *et al.*, 2017). Similarly, it is tempting to hypothesize that Dsc2 may act as a force transducer, mechanosensor, and signaling molecule at DMs in IECs. Further investigations are needed to demonstrate the intrinsic contributions of Dsc2 at DM of IECs and whether Dsc2 modulates Dsg2 function directly or indirectly by influencing Dsg2 stability, turnover rate, and Dsg2-mediated mechanical forces.

In conclusion, we provide new insights supporting a key role for Dsc2 in epithelial barrier function by controlling DM formation and mechanotransduction of tensile forces between epithelial cells.

MATERIALS AND METHODS

Request a protocol through *Bio-protocol*.

Animal experiments

Mice selectively deficient in Dsc2 in the intestinal epithelium were generated by breeding *Dsc2* "floxed" mice with mice expressing the inducible mutated estrogen receptor fused to Cre-recombinase under control of the *Villin* promoter ($Dsc2^{ER\Delta IEC}$) (Flemming, Luissint *et al.*, 2020). Eight-week-old $Dsc2^{ER\Delta IEC}$ and control $Dsc2^{f/f}$ were injected intraperitoneally with 1 mg/100 µl of tamoxifen (T5648, Sigma) dissolved in 10% ethanol and sterile corn oil (C8267, Sigma) for 5 consecutive days. Animals were used 30 d after the last tamoxifen injection. Mice were kept under strict specific pathogen-free conditions with ad libitum access to normal chow and water. All experiments were approved and conducted in accordance with guidelines set by the University of Michigan Institutional Animal Care and Use Committee.

Cell culture and calcium switch assay

SKCO-15 and Caco-2-BBE human model IEC were cultured either on Transwell permeable supports (3 µm pore-size filters, Corning) or on tissue culture-treated plastic as previously described (Ivanov *et al.*, 2007; Nava, Capaldo *et al.*, 2011). KD of Dsc2 was established by RNA interference using short-hairpin RNA (shRNA) specifically

targeting for Dsc2 or scrambled NS control (Kolegraff, Nava *et al.*, 2011a). In short, shRNA transduction (MOI of 2) of IECs was performed in 60–70% confluent IECs using spinfection (1200 × *g* for 30 min at RT), puromycin selection (1 μg/ml) was added during the first split, and cells were grown for minimum of 3 d before experiments to assure proper KD. For cells cultured on Transwell permeable supports, TEER was measured using an EVOM voltmeter with an ENDOHM-12 (World Precision Instruments; Sarasota, FL). Baseline resistance was subtracted from filters covered with cells, and electrical resistance was expressed as $\Omega.cm^2$. For the calcium switch assay, SKCO-15 cells were grown on Transwell permeable supports. The experiment was initiated when TEER reached ~500 $\Omega.cm^2$ by incubation in low calcium media (calcium-free Eagle's minimum essential medium supplemented with 1 μM $CaCl_2$) for 20 h. Then, low calcium media were replaced by normal growth medium (1.8 mM $CaCl_2$) to induce junction reassembly. TEER was monitored for the indicated time and the localization of intercellular proteins was analyzed by immunofluorescence microscopy.

In vitro paracellular flux assay

Paracellular permeability was assessed by 4-kDa FITC-dextran (Sigma-Aldrich; Cat. FD-4) flux through control and Dsc2 KD confluent monolayers were grown on Transwell filters (Costar; Cat. 3450). After TEER measurement, upper and lower Transwell compartments were washed twice and placed with Piruvate buffer (10 mM HEPES, pH 7.4, 1 mM sodium pyruvate, 10 mM glucose, 3 mM $CaCl_2$, and 145 mM $NaCl_2$) for 2 h at 37°C. A freshly prepared solution containing 10 mg/ml 4-kDa FITC-dextran dissolved in Piruvate buffer was added on the top chamber of Transwells for incubation for 2 h at 37°C. Samples from the bottom chamber of the Transwell were collected, and the fluorescence intensity was measured with a fluorescent plate reader (excitation 492 nm; emission 520 nm).

Antibodies

The following primary monoclonal and polyclonal antibodies were used to detect proteins by immunofluorescence or immunoblot analysis: from mouse, anti-human/mouse Dsg2 (clone AH12.2; WB: 1/4,000; IF: 1/400) was generated in-house (Nava, Laukoetter *et al.*, 2007; Kolegraff *et al.*, 2011b); anti-human Dsc2 (Cat. 326200; WB: 1/1000; IF: 1/250) and anti-DPs I/II antibody (clone DP2.15; Cat. ab16434, WB:1/1,000; IF:1/100); from goat, anti-human/mouse E-cadherin (AF748; WB: 1/2,000; IF: 1/400);. from sheep, anti-mouse Dsc2 (Cat. AF7490; IF: 1/200).

From rabbit: anti-Dsg2 (clone EPR6768; WB: 1/1,000; IF: 1/100), anti-DPs I/II antibody (Cat. ab109445; WB: 1/1000, IF: 1/100), anti-Cytokeratin 8 (Cat. ab53280; WB: 1/20,000; IF:1/1,000), and anti-calnexin (Cat. PA5-34665; WB: 1/20,000); anti-glyceraldehyde 3-phosphate dehydrogenase (GAPDH) (Cat. MA5-15738; WB: 1:20.000). Anti-phosphorylated (S2849) DPs I/II antibody (WB: 1/1000; IF: 1/100) was generated in-house (Bouameur *et al.*, 2013; Albrecht, Zhang *et al.*, 2015).

Immunofluorescence microscopy

Cells were grown on glass coverslips and fixed with 4% paraformaldehyde in phosphate-buffered saline (PBS) for 30 min at 4°C followed by permeabilization with 0.5% Triton X-100. Afterward, the cellular epitopes were blocked with 3% bovine serum albumin (BSA; Sigma-Aldrich) for 1 h at room temperature. Cells were incubated overnight at 4°C with primary antibodies diluted in 3% BSA. Cells were then washed five times with PBS+ and incubated for 1 h at room temperature with the following secondary antibodies: donkey antibody against rabbit IgG coupled to Alexa Fluor 488 (Cat. A21206, 1/400) or to Alexa Fluor 555 (Cat. A32794, 1/400); donkey antibody against mouse coupled to Alexa Fluor 488 (Cat. A21202, 1/400) or Alexa Fluor 555 (Cat. A31570, 1/400); donkey antibody against sheep coupled to Alexa Fluor 488 (Cat. A11015, 1/400), and donkey antibody against goat coupled to Alexa Fluor 555 (Cat. A21432, 1/400). Rhodaminated phalloidin (Cat. R415, 1/50) was used for the detection of F-actin. Cells were washed three times, then coverslips mounted onto slide with antifade reagent ProLong Gold (Invitrogen). Fluorescence images were acquired with a microscope Nikon A1 confocal inverted laser microscope or structured illumination superresolution microscope (SIM, Nikon) at the University of Michigan Biomedical Research—Microscopy Core. Fluorescent colocalization analysis was performed using ImageJ software.

Immunoblotting

Western blotting for cell lines and isolated IECs was performed as described previously (Yulis, Quiros *et al.*, 2018). In short, cells were lysed in RIPA (20 mM Tris-Base, 150 mM NaCl, 2 mM EDTA, 2 mM EGTA, 1% sodium deoxycholate, 1% Triton X-100, 0.1% SDS, pH 7.4) containing protease and phosphatase inhibitor cocktails (Sigma-Aldrich) and protein concentration was determined using Pierce Protein BCA kit according to manufacturer's protocol. Samples were boiled for 10 min at 100°C for 10 min in NuPAGE LDS sample buffer (Life Technologies; Eugene, OR) with a final concentration of 100 mM DTT (Sigma-Aldrich) and 20 μg total protein was loaded onto polyacrylamide gels. After electrophoresis, the samples were transferred to a nitrocellulose membrane (Bio-Rad; Hercules, CA) and probed with primary antibodies diluted in 5% nonfat dry milk powder in Tris-buffered saline with 0.1% Tween-20. Membranes were then incubated with appropriate horseradish peroxidase (HRP)–conjugated secondary antibodies for 1 h at room temperature, followed by incubation with a chemiluminescence detection system (Clarity Western ECL Substrate). Finally, membranes were imaged by ChemiDoc imager (Bio-Rad).

Dispase assay

Cell monolayers were treated with 2.4 U/ml Dispase II (Roche Diagnostics, Mannheim, Germany) in PBS with calcium and magnesium at 37°C for 30 min. The cells were then transferred to 15-ml conical tubes containing 5 ml of PBS, which were gently mixed by rotating in a tube rotator 10–30 times. Monolayer fragments were transferred to 12-well tissue culture plates (Corning), imaged using a dissecting microscope, and counted.

In vitro paracellular flux assay

Paracellular permeability was assessed by 4-kDa FITC-dextran (Sigma-Aldrich; Cat. FD-4) flux through control and Dsc2 KD confluent monolayers were grown on Transwell filters (Costar; Cat. 3450). After TEER measurement, upper and lower Transwell compartments were washed twice and placed with piruvate buffer (10 mM HEPES, pH 7.4, 1 mM sodium pyruvate, 10 mM glucose, 3 mM $CaCl_2$, and 145 mM $NaCl_2$) for 2 h at 37°C. A freshly prepared solution containing 10 mg/ml 4-kDa FITC-dextran dissolved in piruvate buffer was added on the top chamber of Transwells for incubation for 2 h at 37°C. Samples from the bottom chamber of the Transwell were collected, and the fluorescence intensity was measured with a fluorescent plate reader (excitation 492 nm; emission 520 nm).

Ileal loop model

In vivo intestinal epithelial permeability at baseline was measured with a previously described intestinal loop model generated in our

laboratory (Monteiro *et al*., 2013; Flemming, Luissint *et al*., 2018). Animals were anesthetized with isoflurane (Fluriso, VETONE) at a constant rate using a rodent anesthesia vaporizer machine (E-Z Anesthesia 7000) and placed on a controlled temperature heat pad to avoid hypothermia. After disinfection of the abdominal skin, laparotomy was performed by midline incision. A 4-cm length of terminal ileum was exteriorized without rupture of the blood supply. The loop was gently flushed with warm HBSS plus calcium and magnesium (HBSS plus; Corning Cellgro) to remove fecal contents and facilitate normalization of volume of contents to allow for comparative analyses between groups. The four generated cut-ends were closed by ligations using nonabsorbable silk suture 3.0 (Braintree Scientific). The loop was injected with 200 µl (1 mg/ml FITC labeled Dextran [4 kDa] dissolved in HBSS+) using the insertion of a 0.5″, 27-gauge needle. The loop was reinserted in the abdominal cavity; then, peritoneum and skin were closed. The surgical procedure lasted approximately 5 min per animal. After 2 h, blood was collected by cardiac puncture prior to euthanasia of the animals by cervical dislocation. FITC-dextran flux was determined by measuring plasma at 488 nm in a microplate spectrophotometer (Epoch Biotek, Vermont) and Gen5 software.

Electron microscopy

Samples were treated as previously described (Palmer *et al*., 2017). Tissues from the terminal ileum were cleared by flushing with HBSS (with calcium) at 37° C and then fixed by vascular perfusion with 2% glutaraldehyde in Gomori phosphate buffer containing 0.1 mM EGTA (pH 7.4) at 37°C. Tissues were excised and cut along the antimesenteric plane, pinned flat in fixative for 10 min at RT, cut into small pieces, and then fixed o/n at 4°C in the same fixative. Tissues were washed in PBS, postfixed in 1% osmium tetroxide in Gomori phosphate buffer pH 7.4 for 1 h at 4° C, washed in distilled water, and then incubated o/n in 2% aqueous uranyl acetate at 4°C. After washes with distilled water, tissues were dehydrated in ethanol (Sigma-Aldrich, Natick, MA) and propylene oxide (Ted Pella, Redding, CA) prior to resin embedding in LX112 resin (Ted Pella). Ultrathin sections were cut with a Leica Ultracut E ultramicrotome (Leica Microsystems, Wetzlar, Germany), placed on formvar and carbon-coated slot grids, and then contrast stained with 2% uranyl acetate and lead citrate. DMs from cells along two villi from each mouse were imaged using a JEOL 1400 electron microscope (JEOL USA, Peabody, MA) equipped with an Orius SC1000 digital CCD camera (Gatan, Pleasanton, CA).

DM structure analysis

DM structure was studied using image analysis software (ImageJ) to measure the width, length, and IMS in electron microscopy images of ileum sections. IMS was generated by an average of the initial, mid, and end distances across DM and, while the width was calculated by subtracting the IMS from the maximal width measurement, the length was obtained by direct measurement.

PCR

Total RNA was extracted from isolated IEC using the RNeasy Kit (QIAGEN) with on-column DNAse I treatment following the manufacturer's protocol. Total RNA (1 µg) was reverse transcribed into cDNA using iScript Reverse Transcription Supermix (Bio-Rad). Gene expression was analyzed by quantitative PCR (qPCR) using SYBR Green (Bio-Rad) with a Bio-Rad CTX Cycler measuring SYBR green incorporation for product detection. Reactions were performed in duplicate with at least five biological replicates. The primers sequence from mouse was: CCTGTCAAGAGCATCCAGTG and GTTATGGTCTGAGCTCGCCATC for Dsg2, ACTGCATGTATTCTGGTACCCTCCA and CGCGCTCAGAATGCTCCTACCC for Dsc2, and GGAATTGTACCGCAGCTTCAAA and GATGACTGCAGCAAATCGCTT for TBP. The relative expression was calculated by the $2^{\Delta\Delta Ct}$ method and normalized to the housekeeping gene TATA box-binding protein (TBP). The fold change was calculated by comparing the values to those obtained on control.

FRET sensors

E-cadherin and Dsg2 FRET sensors are previously described (Borghi, Sorokina, Shcherbakova *et al*., 2012; Baddam, Arsenovic *et al*., 2018). Adenovirus for the E-cadherin and Dsg2 sensors were generated using the AdEasy Adenoviral Vector System (Agilent). The Dsg2 FRET sensor was generated by inserting the TSmod force sensor (Grashoff, Hoffman *et al*., 2010) into human Dsg2 between the transmembrane domain and the ICS site (inserted between Gly762 and Ala763). Adenovirus was used to express the TS in all experiments.

Calcium depletion assay and FRET imaging

Transfected cells expressing the two tension sensor modules (E-cad TSMod and Dsg2 TSMod) were seeded on p-35 20 mm cut-out glass bottom dishes (Celvis) that were precoated with 20 µg/ml fibronectin at room temperature. After 80–90% confluency was reached, the monolayers were washed thoroughly in PBS (no calcium) and incubated in low calcium media at 37°C. After 16–20 h of incubation with low calcium media, the monolayers were replaced with DMEM (1×) supplemented with 10% fetal bovine serum and 5% pen-strep. The monolayers were imaged at 0 and 180 min after calcium repletion and in NT, via live FRET imaging, to study cadherin forces exerted across the epithelial barriers during cell–cell junction recovery. FRET images were acquired using a plan-apochromat 40× water immersion NA 1.1 objective lens on an inverted Zeiss LSM 710 laser scanning microscope (Oberkochen, Germany) at the 458 nm wavelength from an argon laser source.

FRET analysis

The donor and acceptor channels were obtained via spectral unmixing. The acquired intensity images were processed and analyzed with the help of a custom Python code, as previously described (Arsenovic, Ramachandran *et al*., 2016). For each data set, at least 9–10 images were obtained over three independent experiments and were masked manually on ImageJ. The FRET index images were obtained by taking the ratio of the acceptor fluorophore channel to the donor fluorophore channel, which was then multiplied with the binary image masks outlining the cell–cell junctions so as to inspect the FRET pixels of interest. It is noteworthy that only the Dsg2 tension sensor located at cell–cell contacts/ between neighboring cells was analyzed. In addition, the tension sensor is a per molecule estimate of force; therefore, if there is a change in the abundancy of Dsg2, it is not expected to detect a change in the FRET value, unless that was somehow changing the force per molecule.

Subcellular fractionation

Membrane and cytoskeletal fractions were isolated from Dsc2 KD and control SKCO-15 cells by employing a compartmental protein extraction protocol previously described by Bouameur *et al*. (2013). Cells were homogenized in lysis buffer with protease and phosphatase inhibitor cocktails (Sigma-Aldrich; 10 mM Tris, pH 7.5, 5 mM EDTA, 2 mM EGTA, 140 mM $NaCl_2$) containing 1% saponin. Cell lysates were clarified by centrifugation at 4°C at 15,000 rpm for

25 min. Saponin insoluble fraction was solubilized using the lysis buffer containing 1% Triton X-100 (Triton-soluble/membrane fraction) and lysates were centrifuged at 4°C at 15,000 rpm for 25 min. Triton X-100 insoluble fraction was boiled at 95°C for 25 min using the lysis buffer containing 1% SDS (Triton-insoluble/cytoskeletal fraction). The amount of protein was determined using Pierce Protein BCA kit according to manufacturer's protocol and their distributions among the fractions were analyzed by immunoblotting. Na^+/K^+-ATPase and Cytokeratin-8 (CK8) were used as plasma membrane and cytoskeleton markers, respectively. Ponceau S staining was used as a loading control.

Statistics

The statistical significance was measured by two-tailed Student's *t* test, one-way or two-way ANOVA with appropriate multiple comparisons posttest using Graphpad Prism software. A p value ≤ 0.05 was considered significant. Results are expressed as means ± SEM.

ACKNOWLEDGMENTS

The authors thank Roland Hilgarth and Jenna R. Brokaw for technical assistance as well as Kyle H. Smith for his help with the electron microscopy images. The authors also thank the Transgenic and Gene Targeting Core at Emory University, Microscopy and Image Analysis Laboratory and the Unit for Laboratory Animal Medicine (ULAM) at the University of Michigan Medical School. This work was supported by the following grants: Crohn's and Colitis Foundation Research Fellowship no. 623536 (A.R.-S.), German Research Foundation Research Fellowship DFG FL 870/1-1 (S.F.), and the People Program (Marie Curie Actions) of the European Union's Seventh Framework Program (FP7/2007-2013) under REA grant agreement no. 608765 (D.H.M.K.), as well as National Institutes of Health (Musculoskeletal and Skin Diseases) R01 AR041836 and R37 AR43380 (K.J.G.); Harvard Digestive Diseases Center (Microscopy and Histopathology Core B) P30 DK034854 (S.J.H.), R35 GM119617, R03 AR068096 (D.C.), R01 DK61739, DK72564, DK79392 (C.A.P.), R01 DK059888 and DK055679, DK089763 (A.N.); and University of Michigan Center for Gastrointestinal Research (UMCGR) (NIDDK 5P30DK034933).

REFERENCES

Acharya BR, Wu SK, Lieu ZZ, Parton RG, Grill SW, Bershadsky AD, Gomez GA, Yap AS (2017). Mammalian diaphanous 1 mediates a pathway for E-cadherin to stabilize epithelial barriers through junctional contractility. Cell Rep 18, 2854–2867.

Ahmad R, Chaturvedi R, Olivares-Villagómez D, Habib T, Asim M, Shivesh P, Polk DB, Wilson KT, Washington MK, Van Kaer L, *et al*. (2014). Targeted colonic claudin-2 expression renders resistance to epithelial injury, induces immune suppression, and protects from colitis. Mucosal Immunol 7, 1340–1353.

Albrecht LV, Zhang L, Shabanowitz J, Purevjav E, Towbin JA, Hunt DF, Green KJ (2015). GSK3- and PRMT-1-dependent modifications of desmoplakin control desmoplakin-cytoskeleton dynamics. J Cell Biol 208, 597–612.

Andrews C, McLean MH, Durum SK (2018). Cytokine tuning of intestinal epithelial function. Front Immunol 9, 1270.

Arsenovic PT, Ramachandran I, Bathula K, Zhu R, Narang JD, Noll NA, Lemmon CA, Gundersen GG, Conway DE (2016). Nesprin-2G, a Component of the nuclear LINC complex, is subject to myosin-dependent tension. Biophys J 110, 34–43.

Baddam SR, Arsenovic PT, Narayanan V, Duggan NR, Mayer CR, Newman ST, Abutaleb DA, Mohan A, Kowalczyk AP, Conway DE (2018). The desmosomal cadherin desmoglein-2 experiences mechanical tension as demonstrated by a FRET-based tension biosensor expressed in living cells. Cells 7, 66.

Borghi N, Sorokina M, Shcherbakova OG, Weis WI, Pruitt BL, Nelson WJ, Dunn AR (2012). E-cadherin is under constitutive actomyosin-generated tension that is increased at cell-cell contacts upon externally applied stretch. Proc Natl Acad Sci USA 109, 12568–12573.

Bouameur JE, Schneider Y, Begre N, Hobbs RP, Lingasamy P, Fontao L, Green KJ, Favre B, Borradori L (2013). Phosphorylation of serine 4,642 in the C-terminus of plectin by MNK2 and PKA modulates its interaction with intermediate filaments. J Cell Sci 126, 4195–4207.

Broussard JA, Yang R, Huang C, Nathamgari SSP, Beese AM, Godsel LM, Hegazy MH, Lee S, Zhou F, Sniadecki NJ, *et al*. (2017). The desmoplakin-intermediate filament linkage regulates cell mechanics. Mol Biol Cell 28, 3156–3164.

Burdett ID, Sullivan KH (2002). Desmosome assembly in MDCK cells: transport of precursors to the cell surface occurs by two phases of vesicular traffic and involves major changes in centrosome and Golgi location during a Ca(2+) shift. Exp Cell Res 276, 296–309.

Charras G, Yap AS (2018). Tensile forces and mechanotransduction at cell-cell junctions. Curr Biol 28, R445–R457.

Cirillo N (2016). Desmosome assembly, homeostasis, and desmosomal disease. Cell Health Cytoskelet 8, 9–23.

Conway DE, Coon BG, Budatha M, Arsenovic PT, Orsenigo F, Wessel F, Zhang J, Zhuang Z, Dejana E, Vestweber D, *et al*. (2017). VE-cadherin phosphorylation regulates endothelial fluid shear stress responses through the polarity protein LGN. Curr Biol 27, 2219–2225.e5.

el Marjou F, Janssen KP, Chang BH, Li M, Hindie V, Chan L, Louvard D, Chambon P, Metzger D, Robine S (2004). Tissue-specific and inducible Cre-mediated recombination in the gut epithelium. Genesis 39, 186–193.

Fang WK, Liao LD, Zeng FM, Zhang PX, Wu JY, Shen J, Xu LY, Li EM (2014). Desmocollin2 affects the adhesive strength and cytoskeletal arrangement in esophageal squamous cell carcinoma cells. Mol Med Rep 10, 2358–2364.

Farquhar MG, Palade GE (1963). Junctional complexes in various epithelia. J Cell Biol 17, 375–412.

Flemming S, Luissint AC, Kusters DHM, Raya-Sandino A, Fan S, Zhou DW, Hasegawa M, Garcia-Hernandez V, Garcia AJ, Parkos C, Nusrat A (2020). Desmocollin-2 promotes intestinal mucosal repair by controlling integrin-dependent cell adhesion and migration. Mol Biol Cell 31, 407–407.

Flemming S, Luissint AC, Nusrat A, Parkos CA (2018). Analysis of leukocyte transepithelial migration using an in vivo murine colonic loop model. JCI Insight 3.

Fudge D, Russell D, Beriault D, Moore W, Lane EB, Vogl AW (2008). The intermediate filament network in cultured human keratinocytes is remarkably extensible and resilient. PLoS One 3, e2327.

Fujiwara M, Nagatomo A, Tsuda M, Obata S, Sakuma T, Yamamoto T, Suzuki ST (2015). Desmocollin-2 alone forms functional desmosomal plaques, with the plaque formation requiring the juxtamembrane region and plakophilins. J Biochem 158, 339–353.

Godsel LM, Hsieh SN, Amargo EV, Bass AE, Pascoe-McGillicuddy LT, Huen AC, Thorne ME, Gaudry CA, Park JK, Myung K, *et al*. (2005). Desmoplakin assembly dynamics in four dimensions: multiple phases differentially regulated by intermediate filaments and actin. J Cell Biol 171, 1045–1059.

Gosavi P, Kundu ST, Khapare N, Sehgal L, Karkhanis MS, Dalal SN (2011). E-cadherin and plakoglobin recruit plakophilin3 to the cell border to initiate desmosome assembly. Cell Mol Life Sci 68, 1439–1454.

Grashoff C, Hoffman BD, Brenner MD, Zhou R, Parsons M, Yang MT, McLean MA, Sligar SG, Chen CS, Ha T, Schwartz MA (2010). Measuring mechanical tension across vinculin reveals regulation of focal adhesion dynamics. Nature 466, 263–266.

Green KJ, Getsios S, Troyanovsky S, Godsel LM (2010). Intercellular junction assembly, dynamics, and homeostasis. Cold Spring Harb Perspect Biol 2, a000125.

Green KJ, Simpson CL (2007). Desmosomes: new perspectives on a classic. J Invest Dermatol 127, 2499–2515.

Gross A, Pack LAP, Schacht GM, Kant S, Ungewiss H, Meir M, Schlegel N, Preisinger C, Boor P, Guldiken N, *et al*. (2018). Desmoglein 2, but not desmocollin 2, protects intestinal epithelia from injury. Mucosal Immunol 11, 1630–1639.

Gumbiner B, Stevenson B, Grimaldi A (1988). The role of the cell adhesion molecule uvomorulin in the formation and maintenance of the epithelial junctional complex. J Cell Biol 107, 1575–1587.

Harrison OJ, Brasch J, Lasso G, Katsamba PS, Ahlsen G, Honig B, Shapiro L (2016). Structural basis of adhesive binding by desmocollins and desmogleins. Proc Natl Acad Sci USA 113, 7160–7165.

Holthofer B, Windoffer R, Troyanovsky S, Leube RE (2007). Structure and function of desmosomes. Int Rev Cytol 264, 65–163.

Ingber DE (1993). Cellular tensegrity: defining new rules of biological design that govern the cytoskeleton. J Cell Sci 104 (Pt 3), 613–627.

Ingber DE (2003). Tensegrity I. Cell structure and hierarchical systems biology. J Cell Sci 116, 1157–1173.
Ivanov AI, Bachar M, Babbin BA, Adelstein RS, Nusrat A, Parkos CA (2007). A unique role for nonmuscle myosin heavy chain IIA in regulation of epithelial apical junctions. PLoS One 2, e658.
Ivanov AI, Hunt D, Utech M, Nusrat A, Parkos CA (2005). Differential roles for actin polymerization and a myosin II motor in assembly of the epithelial apical junctional complex. Mol Biol Cell 16, 2636–2650.
Khounlotham M, Kim W, Peatman E, Nava P, Medina-Contreras O, Addis C, Koch S, Fournier B, Nusrat A, Denning TL, *et al*. (2012). Compromised intestinal epithelial barrier induces adaptive immune compensation that protects from colitis. Immunity 37, 563–573.
Kimura TE, Merritt AJ, Garrod DR (2007). Calcium-independent desmosomes of keratinocytes are hyper-adhesive. J Invest Dermatol 127, 775–781.
Koeser J, Troyanovsky SM, Grund C, Franke WW (2003). De novo formation of desmosomes in cultured cells upon transfection of genes encoding specific desmosomal components. Exp Cell Res 285, 114–130.
Kolegraff K, Nava P, Helms MN, Parkos CA, Nusrat A (2011a). Loss of desmocollin-2 confers a tumorigenic phenotype to colonic epithelial cells through activation of Akt/beta-catenin signaling. Mol Biol Cell 22, 1121–1134.
Kolegraff K, Nava P, Laur O, Parkos CA, Nusrat A (2011b). Characterization of full-length and proteolytic cleavage fragments of desmoglein-2 in native human colon and colonic epithelial cell lines. Cell Adh Migr 5, 306–314.
Kottke MD, Delva E, Kowalczyk AP (2006). The desmosome: cell science lessons from human diseases. J Cell Sci 119, 797–806.
Kowalczyk AP, Green KJ (2013). Structure, function, and regulation of desmosomes. Prog Mol Biol Transl Sci 116, 95–118.
Kreplak L, Bar H, Leterrier JF, Herrmann H, Aebi U (2005). Exploring the mechanical behavior of single intermediate filaments. J Mol Biol 354, 569–577.
Laukoetter MG, Bruewer M, Nusrat A (2006). Regulation of the intestinal epithelial barrier by the apical junctional complex. Curr Opin Gastroenterol 22, 85–89.
Laukoetter MG, Nava P, Lee WY, Severson EA, Capaldo CT, Babbin BA, Williams IR, Koval M, Peatman E, Campbell JA, *et al*. (2007). JAM-A regulates permeability and inflammation in the intestine in vivo. J Exp Med 204, 3067–3076.
Laukoetter MG, Nava P, Nusrat A (2008). Role of the intestinal barrier in inflammatory bowel disease. World J Gastroenterol 14, 401.
Lechuga S, Naydenov NG, Feygin A, Cruise M, Ervasti JM, Ivanov AI (2020). Loss of β-cytoplasmic actin in the intestinal epithelium increases gut barrier permeability in vivo and exaggerates the severity of experimental colitis. Front Cell Dev Biol 8, 1340.
Lowndes M, Rakshit S, Shafraz O, Borghi N, Harmon RM, Green KJ, Sivasankar S, Nelson WJ (2014). Different roles of cadherins in the assembly and structural integrity of the desmosome complex. J Cell Sci 127, 2339–2350.
Luissint AC, Parkos CA, Nusrat A (2016). Inflammation and the intestinal barrier: leukocyte-epithelial cell interactions, cell junction remodeling, and mucosal repair. Gastroenterology 151, 616–632.
Ma TY (1997). Intestinal epithelial barrier dysfunction in Crohn's Disease. Exp Biol Med 214, 318–327.
Mattey DL, Garrod DR (1986). Splitting and internalization of the desmosomes of cultured kidney epithelial cells by reduction in calcium concentration. J Cell Sci 85, 113–124.
Michels C, Buchta T, Bloch W, Krieg T, Niessen CM (2009). Classical cadherins regulate desmosome formation. J Invest Dermatol 129, 2072–2075.
Monteiro AC, Sumagin R, Rankin CR, Leoni G, Mina MJ, Reiter DM, Stehle T, Dermody TS, Schaefer SA, Hall RA, *et al*. (2013). JAM-A associates with ZO-2, afadin, and PDZ-GEF1 to activate Rap2c and regulate epithelial barrier function. Mol Biol Cell 24, 2849–2860.
Nava P, Capaldo CT, Koch S, Kolegraff K, Rankin CR, Farkas AE, Feasel ME, Li L, Addis C, Parkos CA, Nusrat A (2011). JAM-A regulates epithelial proliferation through Akt/beta-catenin signalling. EMBO Rep 12, 314–320.
Nava P, Laukoetter MG, Hopkins AM, Laur O, Gerner-Smidt K, Green KJ, Parkos CA, Nusrat A (2007). Desmoglein-2: a novel regulator of apoptosis in the intestinal epithelium. Mol Biol Cell 18, 4565–4578.
Naydenov NG, Feygin A, Wang D, Kuemmerle JF, Harris G, Conti MA, Adelstein RS, Ivanov AI (2016). Nonmuscle Myosin IIA regulates intestinal epithelial barrier in vivo and plays a protective role during experimental colitis. Sci Rep 6, 24161.
Nekrasova O, Green KJ (2013). Desmosome assembly and dynamics. Trends Cell Biol 23, 537–546.
Nie Z, Merritt A, Rouhi-Parkouhi M, Tabernero L, Garrod D (2011). Membrane-impermeable cross-linking provides evidence for homophilic, isoform-specific binding of desmosomal cadherins in epithelial cells. Elsevier 286, 2143–2154.
Palmer CJ, Bruckner RJ, Paulo JA, Kazak L, Long JZ, Mina AI, Deng Z, LeClair KB, Hall JA, Hong S, *et al*. (2017). Cdkal1, a type 2 diabetes susceptibility gene, regulates mitochondrial function in adipose tissue. Mol Metab 6, 1212–1225.
Price AJ, Cost AL, Ungewiss H, Waschke J, Dunn AR, Grashoff C (2018). Mechanical loading of desmosomes depends on the magnitude and orientation of external stress. Nat Commun 9, 5284.
Russell D, Andrews PD, James J, Lane EB (2004). Mechanical stress induces profound remodelling of keratin filaments and cell junctions in epidermolysis bullosa simplex keratinocytes. J Cell Sci 117, 5233–5243.
Schlegel N, Meir M, Heupel WM, Holthofer B, Leube RE, Waschke J (2010). Desmoglein 2-mediated adhesion is required for intestinal epithelial barrier integrity. Am J Physiol Gastrointest Liver Physiol 298, G774–G783.
Schlipp A, Schinner C, Spindler V, Vielmuth F, Gehmlich K, Syrris P, Mckenna WJ, Dendorfer A, Hartlieb E, Waschke J, *et al*. (2014). Desmoglein-2 interaction is crucial for cardiomyocyte cohesion and function. Cardiovasc Res 104, 245–257.
Schmitz H, Barmeyer C, Gitter AH, Wullstein F, Bentzel CJ, Fromm M, Riecken EO, Schulzke JD (2000). Epithelial barrier and transport function of the colon in ulcerative colitis. Ann NY Acad Sci 915, 312–326.
Shafraz O, Rubsam M, Stahley SN, Caldara AL, Kowalczyk AP, Niessen CM, Sivasankar S (2018). E-cadherin binds to desmoglein to facilitate desmosome assembly. Elife 7.
Sumigray K, Zhou K, Lechler T (2014). Cell-cell adhesions and cell contractility are upregulated upon desmosome disruption. PLoS One 9, e101824.
Todorovic V, Koetsier JL, Godsel LM, Green KJ (2014). Plakophilin 3 mediates Rap1-dependent desmosome assembly and adherens junction maturation. Mol Biol Cell 25, 3749–3764.
Tornavaca O, Chia M, Dufton N, Almagro LO, Conway DE, Randi AM, Schwartz MA, Matter K, Balda MS (2015). ZO-1 controls endothelial adherens junctions, cell-cell tension, angiogenesis, and barrier formation. J Cell Biol 208, 821–838.
Tsang SM, Brown L, Lin K, Liu L, Piper K, O'Toole EA, Grose R, Hart IR, Garrod DR, Fortune F, Wan H (2012). Non-junctional human desmoglein 3 acts as an upstream regulator of Src in E-cadherin adhesion, a pathway possibly involved in the pathogenesis of pemphigus vulgaris. J Pathol 227, 81–93.
Ungewiss H, Rötzer V, Meir M, Fey C, Diefenbacher M, Schlegel N, Waschke J (2018). Dsg2 via Src-mediated transactivation shapes EGFR signaling towards cell adhesion. Cell Mol Life Sci 75, 4251–4268.
Ungewiss H, Vielmuth F, Suzuki ST, Maiser A, Harz H, Leonhardt H, Kugelmann D, Schlegel N, Waschke J (2017). Desmoglein 2 regulates the intestinal epithelial barrier via p38 mitogen-activated protein kinase. Sci Rep 7, 6329.
Wang L, Llorente C, Hartmann P, Yang AM, Chen P, Schnabl B (2015). Methods to determine intestinal permeability and bacterial translocation during liver disease. J Immunol Methods 421, 44–53.
Yin T, Green KJ (2004). Regulation of desmosome assembly and adhesion. Semin Cell Dev Biol 15, 665–677.
Yulis M, Quiros M, Hilgarth R, Parkos CA, Nusrat A (2018). Intracellular Desmoglein-2 cleavage sensitizes epithelial cells to apoptosis in response to pro-inflammatory cytokines. Cell Death Dis 9, 389.
Zuo L, Kuo W-T, Turner JR (2020). Tight junctions as targets and effectors of mucosal immune homeostasis. Cell Mol Gastroenterol Hepatol 10, 327–340.